SONOPHOTOCATALYTIC DEGRADATION OF PHENOL OVER MAGNETIC SEPARABLE THREE DIMENSIONAL ZnO/Fe_3O_4 HIERARCHICAL HETEROSTRUCTURE UNDER FLUORESCENT LIGHT IRRADIATION

TAN SHAO QI

A project report submitted in partial fulfilment of the
requirements for the award of the degree of
Bachelor of Engineering (Hons) Petrochemical Engineering

Faculty of Engineering and Green Technology
Universiti Tunku Abdul Rahman

April 2018

DECLARATION

I hereby declare that this project report is based on my original work except for citations and quotations which have been duly acknowledged. I also declare that it has not been previously and concurrently submitted for any other degree or award at UTAR or other institutions.

Signature : _____

Name : TAN SHAO QI

ID No. : 13AGB01060

Date : 9 / 4 / 2018

APPROVAL FOR SUBMISSION

I certify that this project report entitled **" SONOPHOTOCATALYTIC DEGRADATION OF PHENOL OVER MAGNETIC SEPARABLE THREE DIMENSIONAL ZnO/Fe_3O_4 HIERARCHICAL HETEROSTRUCTURE UNDER FLUORESCENT LIGHT IRRADIATION"** was prepared by **TAN SHAO QI** has met the required standard for submission in partial fulfilment of the requirements for the award of Bachelor of Engineering (Hons) Petrochemical Engineering at Universiti Tunku Abdul Rahman.

Approved by,

Signature : _____

Supervisor : Dr. Sin Jin Chung_____

Date : 9 / 4 / 2018_____

ACKNOWLEDGEMENTS

First, I would like to thank everyone who had contributed to the successful completion of this project. I would like to express my humblest gratitude to my research supervisor, Dr. Sin Jin Chung for his invaluable advises guidance and his enormous patience throughout the development of the research.

In addition, I would like thank to my friend, Louis Wong Kee Sen who collaborating with me throughout my research work.

Finally, I also would like to express my gratitude to my loving parents and my girlfriend for the physically and mentally support and a lot of encouragement throughout my entire research project.

SONOPHOTOCATALYTIC DEGRADATION OF PHENOL OVER MAGNETIC SEPARABLE THREE DIMENSIONAL ZnO/Fe_3O_4 HIERARCHICAL HETEROSTRUCTURE UNDER FLUORESCENT LIGHT IRRADIATION

ABSTRACT

Water pollution is one of the issues always faced by the world. Phenol reviewed as pollutants due to it have the ability to disrupt human estrogenic activity especially for development and maintenance of female sex characteristics. In recent years, heterogeneous photocatalysis has been widely used for wastewater treatment to degrade the organic compounds as involving phenol. In this study, synthesised of magnetic separable three-dimensional ZnO/Fe_3O_4 hierarchical structures via chemical precipitation-deposition method had been used for sonophotocatalytic degradation of phenol under fluorescent light irradiation and ultrasonic water bath. The synthesised sonophotocatalysts were characterised using X-ray diffraction (XRD), fourier transform infrared spectroscopy (FTIR), scanning electron microscopy (SEM), energy dispersive X-ray spectroscopy (EDX) and photoluminescence spectroscopy (PL). The XRD pattern showed the hexagonal wurzite structure of ZnO that found in the ZnO/Fe_3O_4 sonophotocatalysts. The FTIR spectrum showed the functional group and proved the identity of synthesised ZnO/Fe_3O_4 sonophotocatalysts. The SEM image revealed the sonophotcatalyst in spherical structure as Fe_3O_4 particles deposited close to the ZnO structure. The EDX spectrum revealed the presence of zinc (Zn), Iron (Fe) and oxygen (O) elements existed in the ZnO/Fe_3O_4 sonophotocatalysts. The PL pattern gave information on the electronic structure and evaluated the transition from the excited state to ground state of the synthesised ZnO/Fe_3O_4 sonophotocatalysts. Effect of operating parameters such as initial substrate concentration, ZnO/Fe_3O_4 sonophotocatalyst loading and solution pH were also studied. As the initial phenol concentration increases, the

degradation efficiency of phenol decreased. The optimum ZnO/Fe_3O_4 sonophotocatalyst loading was found to be 1.5 g/L. The optimum initial substrate concentration for sonophotocatalytic degradation was studied to be 20 ppm. The optimum solution pH for sonophotocatalytic degradation of phenol was resulted at pH of 5.

TABLE OF CONTENTS

LIST OF TABLES

LIST OF FIGURES

LIST OF SYMBOLS / ABBREVIATIONS

•OH	Hydroxyl Radicals
3D	Three-dimensional
AOPs	Advanced Oxidation Processes
CB	Conduction Band
CdS	Cadmium Sulphite
e_{CB}^-	Excited Electron
EDX	Energy Dispersion X-ray Spectrum
eV	Electron Volt
Fe_3O_4	Iron (II, III) Oxide
FTIR	Fourier Transform Infrared Spectroscopy
H_2O	Water
H_2O_2	Hydrogen Peroxide
H_2SO_4	Sulfuric Acid
HOO•	Hydroperoxyl Radicals
HPLC	High Performance Liquid Chromatograph
h_{VB}^+	Positive Hole
KI	Potassium Iodide

NaOH	Sodium Hydroxide
O	Oxide
O_2	Oxygen
$O_2^{\bullet -}$	Superoxide Anion Radicals
OH^-	Hydroxyl Ions
PL	Photoluminescene Spectroscopy
SEM	Scanning Electron Microscope
SnO_2	Tin Dioxide
SO_4^-	Sulfate Ions
TiO_2	Titanium Dioxide
TOC	Total Organic Carbon
VB	Valence Band
WO_3	Tungsten Trioxide
XRD	X-Ray Diffraction
Zn	Zinc
$Zn(OH)_2$	Zinc Hydroxide
ZnO	Zinc Oxide
ZnS	Zinc Sulfide

CHAPTER 1

INTRODUCTION

1.1 Background of Study

Into the 21st century, humans were able to proceed further with the coming of industrial revolution as the science became advanced and development of technology rapidly. With all of these improvement science and technology, they brought to an effect of industrial pollution into the natural environments. When most of the factories transformed to the full-scale industry and manufacturing systems, which can lead to a significant and serious issue of increasing pollution level. As Malaysia moving the way towards to the realisation of Vision 2020 to develop the status of becoming an industrial country which resulted an increase of economics due to rapidly growth of industrial development but also led to water pollution problems in the country (Afroz, Hassan and Ibrahim, 2003; Muyibi, Ambali and Eissa, 2007).

According to the report from Department of Environment Malaysia in 2013, a total of 86% of 1.48 million water pollution in Peninsular Malaysia was affected by sewage treatment systems (Ariffin and Sulaiman, 2015). Phenolic compounds presented in industrial effluents such as industrial resin manufacture, coking, coal conversion and petroleum-based processing which have been listed as the main of xenobiotic pollutants (Whiteley and Bailey, 2000). Phenolic compounds reviewed as pollutants due to increase oxygen demand and unpleasant taste in water supplies. The past few decades, it has gathered significant interest for removal of phenol from industrial effluent (Mohler and Jacob, 1957).

Phenol can be known as one of the most common and refractory pollutants produced in the effluent of industrial wastewaters (Augugliaro et al., 1988). Thus, industrial wastewater contained the common contaminant which carcinogenic to living organisms and mammals. Moreover, phenolic compounds are stable and resistance to self degradation in water. They tend to accumulate in soil and groundwater for long period which can sinister to the ecosystem of aquatic living organisms and human health (Pardeshi and Patil, 2008). According to the Central Pollution Control Board 1992 of environment protection rules, the discharge limit of phenols in inland water was 1 mg/L (Lathasree et al., 2004). The degradation of phenols compounds has been studied by conventional chemical, physical and biological methods. A proper treatment of phenolic compounds is urgently required before their continuous discharge into the environment which can affect the aquatic living organisms and human health.

Recently, Advance Oxidation Processes (AOPs) are one of the promising methods that have been widely used in treating and reducing organic pollutants in wastewater treatment. The function of AOPs can reduce the contaminants concentration lower than 5 ppb from hundreds ppm. Thus, this process was named as '*water treatment processes of the 21st century*'. Furthermore, dissolved organic contaminants can be broken down by AOPs as demonstrated that constant rate of contaminant with hydroxyl radicals (•OH) was proportional to destruction rate of contaminant (Munter, 2010). The AOPs methods included ultrasonic (US), ultraviolet (UV), hydrogen peroxide, electrochemical oxidation, photocatalysis, ozonation and Fenton's process can be used to generate the free hydroxyl radicals (•OH) for organic pollutants degradation (Tabasideh et al., 2017). These methods have difference of reacting system but the produced •OH radicals were highly reactive oxidizing agents (Asghar, Abdul Raman and Wan Daud, 2015).

One such method within the AOPs, namely heterogeneous photocatalysis that can degrade organic and inorganic pollutants over different types of semiconductors which are titanium dioxide (TiO_2), zinc oxide (ZnO), zirconium dioxide (ZrO_2) and tin dioxide (SnO_2) (Pardeshi and Patil, 2008). Moreover, heterogeneous photocatalysis was an effective choice due to environmentally friendly process by mineralizing the organic pollutants into carbon dioxide and water (Zangeneh et al.,

2015). However, photocatalytic degradation rate can be affected when the pollutants deposited on the surface which blocked active sites (May-Lozano et al., 2017). Hence, photocatalysis needed to combine with some other synergistic processes to clean the surface of active sites during the process while one of the techniques will be ultrasonic irradiation (Hu et al., 2014).

Ultrasonic irradiation can be considered as one of the effective ways for degradation of hazardous organic compounds in water (Tabasideh et al., 2017). Oxidation of the substrate and degradation intermediates are the main responsible for the observed synergy which induced by the increased amount of reactive radical species in sonolysis (Salavati, Tavakkoli and Hosseinpoor, 2012). However, complete degradation was not occurred by ultrasonic degradation due to time consuming and consumed vast amounts of energy (Khataee et al., 2017). Nevertheless, combination of ultrasonic (US) and ultraviolet (UV) irradiation had synergistic affect that can accelerate the catalytic degradation organic compounds from water (Khataee, Arefi-Oskoui and Samaei, 2018). The limitation of degradation efficiency can also be overcame by applying semiconductors catalyst for the processes (Tabasideh et al., 2017).

Titanium dioxide (TiO_2) has been selected for degradation of pollutants due to its efficient electron transfer to molecular oxygen, high photosensitivity and nontoxic nature (Xia et al., 2011). On the other hand, ZnO was recorded as more suitable photocatalysts for semiconductor photodegradation mechanism compared to TiO_2 due to the ZnO was more economical and sometimes even more efficient (Daneshvar, Salari and Khataee, 2004). ZnO has been used in various areas, such as electrical, electromagnetic shielding, biosensors, gas sensors and elimination of organic pollutants (Hong et al., 2008). In recent wastewater treatment processes, application of ZnO with three-dimensional (3D) complex hierarchical structure is more acceptable than the low dimensional ZnO due to its lower density, higher surface area, higher surface permeability and better photocatalytic behaviour (Xu, Ao and Chen, 2009).

Three-dimensional (3D) hierarchical structure had excellent properties for potential applications in the bottom-up fabrication of functional devices including photocatalysts, sensors and drug release systems. Moreover, it has been demonstrated to show enhanced photocatalytic performance from three-dimensional (3D) hierarchical structure including dandelion-like, flower-like and seaurchin shaped (Sun et al., 2012). The characteristics of three-dimensional (3D) of ZnO having a significant increase the efficiency of degradation processes (Wang et al., 2005). However, single semiconductor suffered ineffective separation method could result in low harvest of visible light, poor selective adsorption, photocatalyst deactivation and loss of the catalysts (Xia et al., 2011).

Recently, synthesis of magnetic separable iron (III) oxide/zinc oxide (Fe_3O_4/ZnO) nanocomposites has been designed and developed in order to improve the photocatalytic activity of semiconductor (Saffari et al., 2015). It is an effective way to solve the problems, as Fe_3O_4/ZnO nanocomposites can separate easily from the solution with an external magnet (Xia et al., 2011). Moreover, Fe_3O_4 has attracted interest due to its electric and magnetic properties with the transfer of electron between Fe^{2+} and Fe^{3+} at octahedral sites. Magnetite nanoparticles contain some unique properties including degradation of organic pollutants, suitable for mechanical hardness and good chemical stability which suitable to be used in nanocomposite photocatalysts (Saffari et al., 2015).

1.2 Problem Statements

In recent years, intensification of industrial activities was being known as one of the major problems in modern society (Souza et al., 2016). Furthermore, growth of population and increasing industrial productivity became the main issue of natural water sources contamination (Souza et al., 2016). From the industrial processes, phenols are being produced through various anthropogenic inputs into the environment. The toxicity, bio-accumulative and persistence of produced phenols in wastewater effluent have intensified concern impact the health of living organisms and may pose serious threat to public health (Zhong et al., 2010). Phenol present as a large group of the high solubility, strong reactivity and poor biodegradation in water

(Zhang et al., 2004). Even phenol is at low concentrations, the toxicity level will never be reduced. Besides, phenols are able to disrupt human estrogenic activity especially for development and maintenance of female sex characteristics (Zhong et al., 2010). According to Busca et al (2008), phenols existed in wastewater from different industries which reported as refineries (6–500 mg/L), coking operations (28–3900 mg/L), coal processing (9–6800 mg/L), and manufacture of petrochemicals (2.8–1220 mg/L). In other sources of waste stream water containing phenols were pharmaceutical, plastics, wood products, paint, and pulp and paper industries (0.1–1600 mg/L). Therefore, it is needed to remove of organic pollutants from wastewater effluent to reduce the risk of water pollution. (Ahmed et al., 2010).

Heterogeneous photocatalysis is one of the efficient advanced oxidation processes (AOPs) that able to mineralise the organic pollutants followed by extremely efficient degradation efficiency, fast reaction speed, mild react conditions, good selectivity and non hazardous (Vaiano et al., 2018). AOPs have the ability for removing the organic compounds in the water by oxidation mechanism that relied on hydroxyl radical (•OH) formation (Salim et al., 2018). However, the mass transfer limitations and the blockage of active sites by adsorbed pollutants caused the photocatalysts became less efficient during continuous operation (May-Lozano et al., 2017). Hence, ultrasonic irradiation can be one of such techniques which can clean up the active sites by acoustic cavitation phenomena (ElShafei et al., 2018).

Ultrasonic high-frequency waves are used as the production of the cavitation phenomenon and microbubbles (Khataee et al., 2017). In general, three repetitive steps for the cavitation phenomenon are production, rapid growth and implosion of the microbubbles in liquid (Khataee, Arefi-Oskoui and Samaei, 2018). The phenomenon can be known as acoustic cavitation that can produce physical environments and unequal chemical (Tabasideh et al., 2017). However, high energy demand and long treatment period are not occurred by using application of sonolysis alone in large-scale wastewater treatment plant (Sajjadi, Khataee and Kamali, 2017). Thus, combination of photocatalysis and ultrasonic irradiation was found to accelerate degradation and mineralisation rate of organic compounds due to the increase in the generation of ·OH radicals (Ahmad et al., 2014; ElShafei et al., 2018)

Titanium dioxide (TiO_2) has been introduced in many studies which can use as catalyst for treating wastewater containing organic pollutants (Souza et al., 2016). TiO_2 has strong oxidizing power, low toxicity, low operation temperature, high photocatalytic activity, low energy consumption, large availability, water insolubility and high chemical stability (Wang et al., 2005; Mu et al., 2010). In recent years, zinc oxide (ZnO) can replace TiO_2 due to similar mechanism for photocatalytic degradation of pollutants, high catalyst efficiency, low cost, non-toxic and chemical stability (Daneshvar, Salari and Khataee, 2004; Souza et al., 2016). ZnO had the same band gap as TiO_2 that can form electron-hole pairs to undergo redox reactions (Lam et al., 2012). Therefore, ZnO semiconductor applied in application became more economical as compared to TiO_2 for large scale photocatalytic degradation.

According to Mohajerani, Lak and Simchi (2009), surface area and electronic structure of material can affect by the photocatalytic process, which depended on the structural characteristics. Low dimensional nano-scaled building block such as nanowires, nanorods, nanofilms and nanopellets have been prepared successfully for photocatalytic processes (Dong et al., 2011). The 3D hierarchical structure was introduced from the surfactants or structure directing reagents assisted assembly mechanism and self-assembly of nano-scaled building blocks (Sin et al., 2013). Consequently, three-dimensional (3D) ZnO hierarchical structure was introduced to avoid the aggregate of low dimensional nano-scaled building block with great concern of low density, high surface area, surface permeability and good photocatalytic behaviour (Dong et al., 2011). Moreover, 3D ZnO hierarchical structure also improved the uniformity of the active sites distribution and provided abundant active adsorption sites and photocatalytic reaction sites (Xia et al., 2016).

At present, there are some restricting applications of ZnO in photocatalytic processes. One of the drawbacks is the difficulty in separation of photocatalysts from the treated solutions which leading to increase the cost of the processes and may lead to secondary pollution due to loss of photocatalyst (Guo et al., 2011; Shekofteh-Gohari and Habibi-Yangjeh, 2016). Instead of using pure ZnO semiconductor, photocatalysts with magnetic properties showed the advantages such as low operational costs, short separation time, and simple technical requirements (Habibi-Yangjeh and Shekofteh-Gohari, 2016). Hence, magnetically separable visible-light-

driven photocatalysts were prepared by incorporating a magnetic component into the photocatalytically active materials (Shekofteh-Gohari and Habibi-Yangjeh, 2016). A magnetic component with separation function and a photocatalytic component with photocatalytic function are the two functional parts for a synthesised magnetic photocatalysts (Chalasani and Vasudevan, 2013; Feng et al., 2014; Sun et al., 2014). Magnetic separable ZnO/Fe_3O_4 photocatalysts in photocatalytic degradation can separate effectively and owned the recyclability function (Shylesh, Schünemann and Thiel, 2010).

1.3 Objectives

The objectives of this research are:

1. To synthesise the magnetic separable ZnO/Fe_3O_4 photocatalysts via a surfactant free chemical precipitation-deposition method.
2. To characterise the physical, chemical and optical properties of the synthesised photocatalysts.
3. To study the sonocatalytic, sonophotocatalytic and photocatalytic degradation of phenol over the synthesised photocatalysts.

1.4 Scope of Study

This study focused on the sonophotocatalytic, photocatalytic and sonocatalytic and degradation of phenol with the use of 3D ZnO hierarchical structures coupled with Fe_3O_4 (ZnO/Fe_3O_4) as photocatalysts. The ZnO photocatalyst is synthesised by chemical precipitation method without using any surfactant. Then, ZnO/Fe_3O_4 is produced by depositing Fe_3O_4 on synthesised ZnO. The prepared catalysts are characterised with X-ray diffraction (XRD), scanning electron microscope (SEM), energy dispersive X-ray spectroscopy (EDX), fourier transform infrared spectroscopy (FTIR) and photoluminescence (PL) spectroscopy. Lastly, the performances of the synthesised ZnO/Fe_3O_4 nanocomposites are evaluated by degradation of phenol via sonocatalytic, photocatalytic and sonophotocatalytic reactions.

CHAPTER 2

LITERATURE REVIEW

2.1 Advanced Oxidation Process (AOP)

Advance Oxidation Processes (AOPs) involved photocatalysis, catalytic wet peroxide oxidation, hydrogen peroxide, ozone and Fenton's reagent with or without ultraviolet light (Pardeshi and Patil, 2008). AOPs can be applied to treat wastewaters to obtain the reaction byproducts having a higher biodegradability and lower toxicity compared to the parent compounds. AOPs of biological processes can be applied at post-treatment or pre-treatment as the byproducts are less biodegradable and more toxic than parent pollutants (Ribeiro et al., 2015). These processes can be characterised by •OH radicals with redox potential of 2.80 eV which known as highly reactive oxidizing agent (Asghar, Abdul Raman and Wan Daud, 2015). •OH radicals are low selectivity and highly reactive, leading to attack the most part of organic molecules (Andreozzi, 1999).

AOPs can be divided into electro-chemical, sono-chemical, non-photochemical and photochemical processes that concerning the methodology to generate •OH radicals (Ribeiro et al., 2015). Non-photochemical AOPs generated •OH radicals without using light energy. For example, ozone with hydrogen peroxide at elevated values of pH (>8.5) and ozone with Fe^{2+} as the catalyst in ozone/Fenton system (Munter, 2010). On the other hand, photochemical AOPs are light induced reactions to generate •OH radicals by the combination of oxidants or semiconductors (Agustina, Ang and Vareek, 2005).

Heterogeneous photocatalysis is one of the photochemical AOPs, which makes use the semiconductor slurries for catalysts such as TiO_2/UV and ZnO/UV (Agustina, Ang and Vareek, 2005; Ribeiro et al., 2015). Characterisation can be applied at the active sites of the catalyst surface that happened on the adsorption of reactants and desorption of products. Wastewater pollutants can be destructed by the attributes of •OH radical and transformed them to less non-toxic products (Huang, Dong and Tang, 1993). AOPs can act as the clean technologies for water pollutant treatment when the contaminants and reaction intermediate products can be completely mineralised and non secondary wastes were generated. Hence, no final disposal and post treatment were required for AOPs (Ribeiro et al., 2015).

2.2 Principle of Sonophotocatalysis

In photocatalytic process, strong oxidizing •OH radical was produced by the ability of the photocatalysts when irradiated with UV light and sunlight (Yasmina et al, 2014). Photocatalysis drives the oxidation process by reacting with the pollutants in the environment resulting to the degradation and complete mineralisation of organic and inorganic pollutants if the treatment time is adequate due to the in-situ generation of reactive •OH radicals (Tokode et al., 2016).

Heterogeneous photocatalysis has been discovered in 1972s by Fujishima and Honda after the electrochemical photolysis of water at a TiO_2 electrode was reported. Usage of TiO_2 and platinum electrodes without current applied, water molecules were decomposed into oxygen and hydrogen by visible light (Linsebigler, Lu and Yates, 1995). The most commonly used photocatalysts are titanium dioxide (TiO_2), zinc oxide (ZnO), zirconium dioxide (ZrO_2) and cadmium sulfide (CdS) (Pardeshi and Patil, 2008).

Generally, heterogeneous photocatalysis is started via absorption of photons on the surface of the catalyst (Ribeiro et al., 2015; Yasmina et al, 2014). When suitable wavelength of the light illuminated the catalyst, an electron from the valence band promoted to the conduction band. It can cause an excess of negative charge in

the conduction band and leaving in the valence band. The separated electron-hole pairs participated in redox reactions and equivalents respectively of oxidizing and reducing (Kwon, 2004). Water molecules adsorbed on the active sites of the semiconductor can reduce the hole, leading to the formation of •OH radicals (Yasmina et al, 2014; Kwon, 2004).

On the other hand, the sonocatalysis and sonophotocatalysis with ultrasonic irradiation have emerged for a wide application on the treatment and degradation of refractory compounds (Li et al., 2018). Ultrasonic degradation of organic pollutants concerned the acoustic cavitation which generated from the ultrasonic irradiation (Khataee et al., 2018). The ultrasound included of three stages: nucleation, expansion and implosion of cavitation bubbles, resulting in very high temperature and high pressure about 5000k and 1000atm (Khataee, Hassandoost and Rahim Pouran, 2018). Consequently, the extreme situation generated from the conversion of water molecules to H• and •OH radicals by local hot spots at the bubble liquid interface (Sajjadi, Khataee and Kamali, 2017). This violent situation caused the pyrolysis of (H_2O) into extremely reactive hydrogen atoms (H•), hydroxyl radicals (•OH) and oxygen atoms (O•) (Sajjadi, Khataee and Kamali, 2017). The reactions are shown in Equations 2.1 – 2.2 (Sajjadi, Khataee and Kamali, 2017).

$$H_2O + \text{Ultrasonic irradiation} \rightarrow \bullet OH + H \quad (2.1)$$

$$\bullet OH + \bullet OH \rightarrow H_2O_2 \quad (2.2)$$

The superoxide anion radicals ($\bullet O_2^-$) can be formed due to the attack of electron to adsorbed oxygen on the catalyst surface (Ribeiro et al., 2015). Radical oxidations led to the degradation process due to the initiation of strong oxidants. Degradation of organic pollutants by the reactive radicals on the catalyst can eventually generate the non-toxic mineral species as intermediate products (Zangeneh et al., 2015).

2.2.1 Zinc Oxide as Sonophotocatalyst

Zinc Oxide can be obtained in three types of crystal structures which are hexagonal wurtzite, cubic rocksalt and cubic zincblende (Özgür et al., 2005). The three crystal structures model of ZnO are shown in Figure 2.1. ZnO is an oxidic compound which appears as white hexagonal crystal and white powder with the name of zinc white. Hexagonal wurtzite structure of ZnO is the most suitable structure due to the thermodynamically stable phase at ambient conditions (Özgür et al., 2005). However, cubic rocksalt structure can be obtained at high pressures (~9 GPa at 300K) and the cubic zincblende structure can be occurred under the conditions through epitaxial growth of ZnO on cubic substrates. This is the reason of hexagonal wurtzite structure being focused in sonophotocatalytic studies due to cubic rocksalt structure and cubic zincblende structure only can occur under certain situations (Lam et al., 2012).

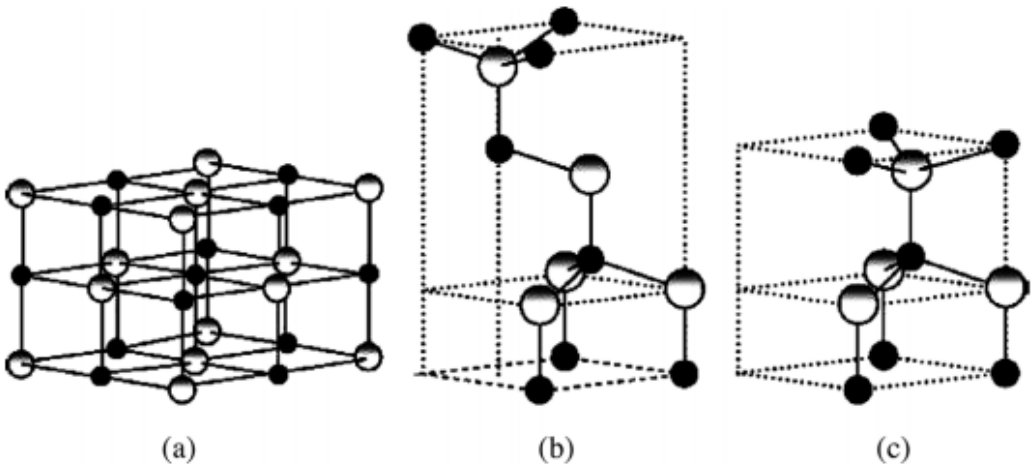

Figure 2.1: Stick and Ball Representation of ZnO Crystal Structures: (a) Cubic Rocksalt; (b) Cubic Zincblende; (c) Hexagonal Wurtzite. The Shaded White and Black Spheres Denote Zn and O Atoms, Respectively (Özgür Et Al., 2005).

Besides, ZnO has bitter taste, odourless, insoluble in water and low hardness at the ranged from 4 to 5 GPa (Lee et al., 2016). ZnO has been applied in sonophotocatalysis and has emerged as the leading candidate due to environmental friendly and excitonic emission processes (Lee et al., 2016). ZnO has also demonstrated to be more applicable and efficient than TiO_2 for sonophotocatalytic

degradation and complete mineralisation of environmental pollutants (Lam et al., 2012).

The band gap positions of some common semiconductors are shown in Figure 2.2 (Xie et al., 2016). Both TiO_2 and ZnO having similar band gap and expected to have similar photocatalytic capability. The largest advantage of ZnO as photocatalysts compared to TiO_2 is the ability to absorb a huge range of solar spectrum (Lee et al., 2016). Furthermore, ZnO is relatively cheaper compared to TiO_2 due to ZnO is more economical for large scale water treatment operations (Daneshvar et al., 2007; Lee et al., 2016).

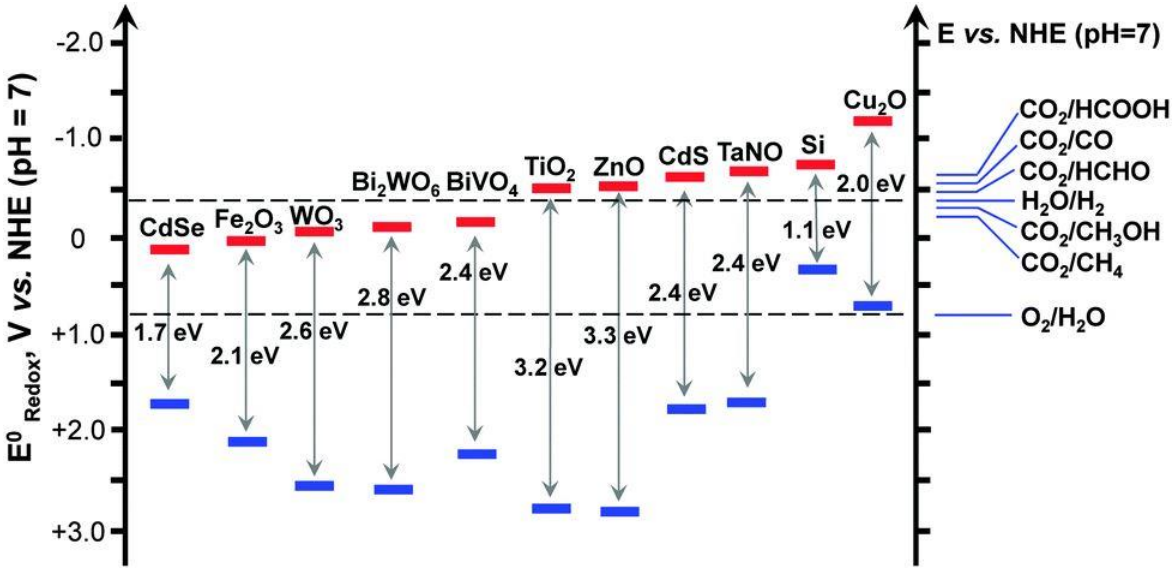

Figure 2.2: Band gap positions of some typical semiconductor photocatalysts (Xie et al., 2016).

2.2.2 Mechanism of Zinc Oxide Sonophotocatalyst

ZnO particle with energies for photocatalytic reactions initiated by the absorption radiation having larger than its band gap energy from the illumination and photo-excitement of valence band electrons obtained which resulting in electron hole pairs (Ribeiro et al., 2015). The electrons (e_{CB}^-) of ZnO will be promoted from valence band to conduction band as long as the ultraviolet light energy was larger than ZnO band gap energy. The surface of ZnO particle formed positive hole (h_{VB}^+) and electron (e_{CB}^-) (Lee et al., 2016). The mechanism of generated electron (e_{CB}^-) and positive hole (h_{VB}^+) on the surface of ZnO is shown in Equation 2.3 (Lee, Abd Hamid and Lai, 2015).

$$\mathrm{ZnO} + h\nu \rightarrow \mathrm{ZnO}\,(e_{CB}^- + h_{VB}^+) \tag{2.3}$$

The photogenerated charge carriers (e_{CB}^- and h_{VB}^+) can recombine with each other in valence band and dissipated in the form of heat. However, it can also be involved in oxidation and reduction reactions on the catalyst surface (Tokode et al., 2016). The mechanisms are shown in Equations 2.4 – 2.6 (Lee et al., 2016). The positive hole (h_{VB}^+) is a potent oxidizing agent that can oxidise hydroxyl ions (OH^-) to form hydroxyl radical (•OH) (Mahmoud and Fouad, 2015; Lam et al., 2012).

$$e_{CB}^- + h_{VB}^+ \rightarrow \text{heat} \tag{2.4}$$

$$h_{VB}^+ + OH^- \rightarrow \bullet OH \tag{2.5}$$

$$h_{VB}^+ + H_2O^- \rightarrow H^+ + \bullet OH \tag{2.6}$$

To prolong the recombination, one of the electron (e_{CB}^-) acceptors such as oxygen can be used as electron scavengers to form the superoxide anion radicals ($\bullet O_2^-$). The reaction is shown in the Equation 2.7 (Lee et al., 2016).

$$e_{CB}^- + O_2 \rightarrow \bullet O_2^- \tag{2.7}$$

Moreover, the formed $\bullet O_2^-$ can be further protonated to obtain hydroperoxyl radical (HOO•) and finally formed hydrogen peroxide (H_2O_2). The following

photocatalytic reactions (Equation 2.8 – 2.11) showed the generation of hydroxyl radicals (•OH) (Lee et al., 2016; Tokode et al., 2016; Lam et al., 2012). Figure 2.3 shows the general mechanism of photocatalytic degradation (Daneshvar, Salari and Khataee, 2004).

$$\bullet O_2^- + H^+ \rightarrow HOO\bullet \quad (2.8)$$

$$2\ HOO\bullet \rightarrow H_2O_2 + O_2 \quad (2.9)$$

$$H_2O_2 + \bullet O_2^- \rightarrow \bullet OH + OH^- + O_2 \quad (2.10)$$

$$H_2O_2 + e_{CB}^- \rightarrow OH^- + \bullet OH \quad (2.11)$$

Heterogeneous nucleation of bubble can increase the formation of cavitation bubbles by generating hot spots in the solution (Darvishi Cheshmeh Soltani et al., 2016). H_2O molecules will pyrolyse to form •OH radicals due to the generated hot spots in the solution (Zhu et al., 2012). Sonication involves UV light that ZnO particles can be excited to use as photocatalysts (Darvishi Cheshmeh Soltani et al., 2016). Degradation of organic compounds in sonolysis involved collapsing cavitation bubbles in a high temperature and pressure (Darvishi Cheshmeh Soltani et al., 2016). Moreover, US irradiation can also produce electron-hole pairs of •OH radicals and superoxide anions $\bullet O_2^-$ when catalyst is added which can degrade and mineralise to CO_2 and H_2O (Zhu et al., 2012). The mechanisms are shown in Equations 2.12 – 2.16 (Zhu et al., 2012).

$$H_2O + \text{ultrasound} \rightarrow \bullet OH + \bullet H \quad (2.12)$$

$$\text{Catalyst} + \text{ultrasound} \rightarrow e^- + h^+ \quad (2.13)$$

$$e^- + O_2 \rightarrow \bullet O_2^- \quad (2.14)$$

$$h^+ + H_2O \rightarrow \bullet OH \quad (2.15)$$

$$\text{Catalyst} + \text{ultrasound} + H_2O + O_2 + \text{Phenol} \rightarrow CO_2 + H_2O \quad (2.16)$$

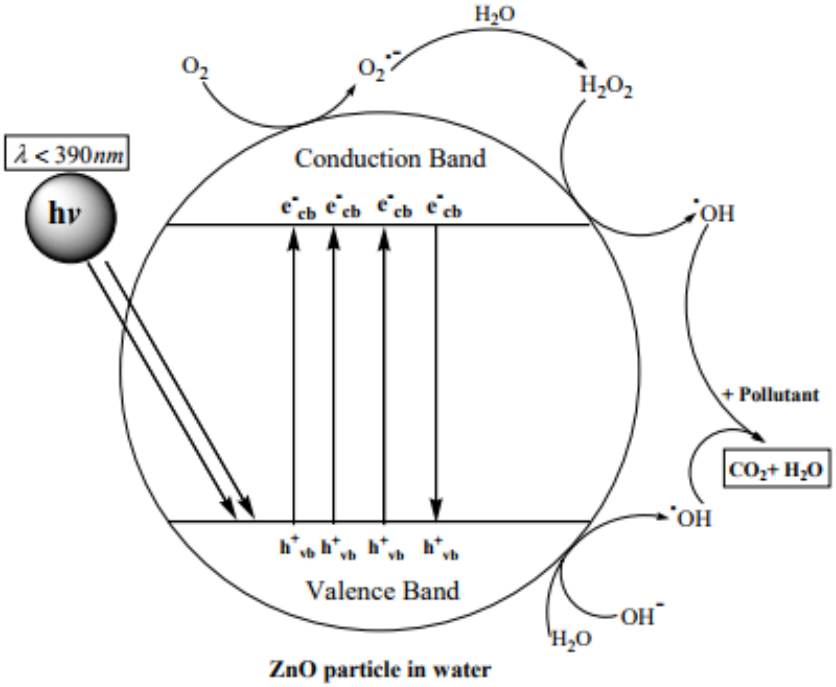

Figure 2.3: General Mechanism of Photocatalysis (Daneshvar, Salari and Khataee, 2004).

2.3 Three-Dimensional (3D) Structure of ZnO

The fabrication of three-dimensional (3D) structure is getting attention due to the characteristics of high surface area, low density, good surface permeability and efficient light harvesting efficiencies (Xu, Ao and Chen, 2009). Photocatalytic activity can be affected by specific surface area and porous structure of photocatalyst (Zhao et al., 2014). High surface-to-volume ratios of hierarchical nanostructures provided adsorption of active sites onto the surface of ZnO for photocatalytic reaction (Mukhopadhyay et al., 2015). Therefore, photocatalytic efficiency can be improved by increasing the surface area of photocatalyst (Zhao et al., 2014).

Casillas et al. (2017) carried out an experiment on the photocatalytic degradation of phenol using Al_2O_3-Nd_2O_3-ZnO composites. Al_2O_3-Nd_2O_3-ZnO composites with different specific surface areas of 272, 243, 232, 137m^2/g were added into phenol and irradiated under visible light irradiation within 3 hours. The results showed that the Al-Nd-Zn composites with highest specific surface area (272 m^2/g) has the highest degradation percentage of 90%, while the Al-Nd-Zn composite with the lowest specific surface area (137 m^2/g) decreased significantly for degradation efficiency. The relationship between the specific surface area of photocatalyst with photocatalytic activity have been clearly shown.

Enhancement of specific surface area can also be formed by synthesizing different morphologies of catalysts. Many morphologies of ZnO have been synthesised such as nanobelts, nanotubes, nanowires and nanocombs. However, it is still exhibited lower photocatalytic efficiency for low dimensional nanoscaled building blocks due to the greater chances of aggregation in photocatalysis and synthesis processes which can cause reduction of photocatalytic efficiency and specific surface area (Zhao et al., 2014). Three-dimensional structure (3D) catalysts contained more reaction at the active sites and enhanced the segregation efficiency for e_{CB}^- and h_{VB}^+ due to larger surface area (Lee et al, 2016). Therefore, increment of photocatalytic degradation due to enhancement of catalytic activity (Lei et al., 2012).

Moreover, hierarchical structures of ZnO can be constructed by multiple techniques, for example precipitation, sol-gel, hydrothermal, electro-deposition,

chemical vapour deposition, ultrasonic and microemulsion (Li and Haneda, 2003). For the preparation of ZnO hierarchical structures, precipitation is most suitable and economical method which applied chemical reactions between the reactants. No-requirement of high cost for special apparatus and environment friendly in reactant preparation the advantages in precipitation method (Kahouli et al., 2015).

2.4 Modification of ZnO Sonophotocatalysts via Fe_3O_4 Coupling

ZnO sonophotocatalysts are eco-friendly, nontoxic, thermal and chemical stable, non-corrosive and having a great degradation capacity for wastewater treatment (Abazari, Mahjoub and Sanati, 2016). However, it is difficult to recover and separate the catalysts from the aqueous solutions in the way of cost-efficiently and straight forwardly. Hence, the remained catalysts could be generated secondary pollution (Shekofteh-Gohari and Habibi-Yangjeh, 2015). The suspended particles can be separated from the suspension after complicated centrifugation and filtration processes (Abazari, Mahjoub and Sanati, 2016). Recently, magnetically separable sonophotocatalysts which can be separated via external magnetic force could eliminate the complicated separation steps when recovering the catalysts (Shekofteh-Gohari and Habibi-Yangjeh, 2015).

Magnetically separable sonophotocatalysts with distinct advantages in terms of high speed, short operation times, and low cost which can be known as effective strategy for magnetic separation of sonophotocatalysts from treated solutions. The sonophotocatalysts with magnetic properties provided a convenient approached for separation of sonophotocatalysts from a large amount of wastewater within a short time using external magnetic force (Shekofteh-Gohari and Habibi-Yangjeh, 2016). The application of magnetic separation is to increase catalytic reusability and prevented the agglomeration and loss of catalysts. The listed ferromagnetism advantageous materials are iron oxides, which subsume maghemite (γ- Fe_2O_3) and magnetite (Fe_3O_4). Maghemite (γ-Fe_2O_3) and magnetite (Fe_3O_4) can be unstable crystal structure iron oxide that faced the risk of conversion. The problem can be overcome by introducing of ZnO (Abazari, Mahjoub and Sanati, 2016).

Iron (II, III) Oxide (Fe_3O_4) is the important member of spinel type ferrite which utilised in synthesizing the magnetically separable catalysts (Hong et al., 2008). Iron (II, III) Oxide (Fe_3O_4) magnetic nanoparticles can be known as non-toxic, biocompatible, superparamagnety, high coercivity and low curie temperature (Wei et al., 2012). ZnO/Fe_3O_4 nanocomposite sonophotocatalysts have better sonophotocatalytic performance and more photostable compared to ZnO (Suresh and Karthikeyan, 2016). Fe^{3+} dopants can utilise the visible light to photocatalyse the degradation of pollutants and involved in separation of photo-generated electrons and holes. Hence, Fe^{3+} can act as a temporary photo-generated electron or hole-trapping site to prolong their lifetime and inhibited the recombination of photo-generated charge carriers (Yu, Xiang and Zhou, 2009). Fe^{3+} is more stable as compared to Fe^{4+} and Fe^{2+} half-filled d orbital (d^5) (Ambrus et al., 2008). The electron configurations of Fe^{2+}, Fe^{3+} and Fe^{4+} are shown as Figure 2.4 (Yu, Xiang and Zhou, 2009). Besides, Fe^{2+} or Fe^{4+} was able to transfer the trapped charge carriers to the adsorbed oxygen (O_2) and surface hydroxyl (-OH) for regenerate Fe^{3+}. The reactions are shown in Equations 2.17 – 2.20 (Yu, Xiang and Zhou, 2009).

$$Fe^{3+} + e^{+} \rightarrow Fe^{2+} \quad (2.17)$$

$$Fe^{2+} + O_2 \rightarrow Fe^{3+} + O_2^{-} \quad (2.18)$$

$$Fe^{3+} + h^{+} \rightarrow Fe^{4+} \quad (2.19)$$

$$Fe^{4+} + OH^{-} \rightarrow Fe^{3+} + \bullet OH \quad (2.20)$$

On the other hand, during the sonophotocatalytic process, surface oxygen vacancies can trap photoinduced electrons which to inhibit the recombination of photogenerated electron–hole pairs. Oxygen species such as O_2 and OH^- were able to absorb by surface oxygen vacancies easily. Hence, the oxygen species were transformed into $\bullet O_2^-$ and •OH for degradation of various organic pollutants into carbon dioxide (CO_2) and water (H_2O) after react with photogenerated carriers (Wang et al., 2016).

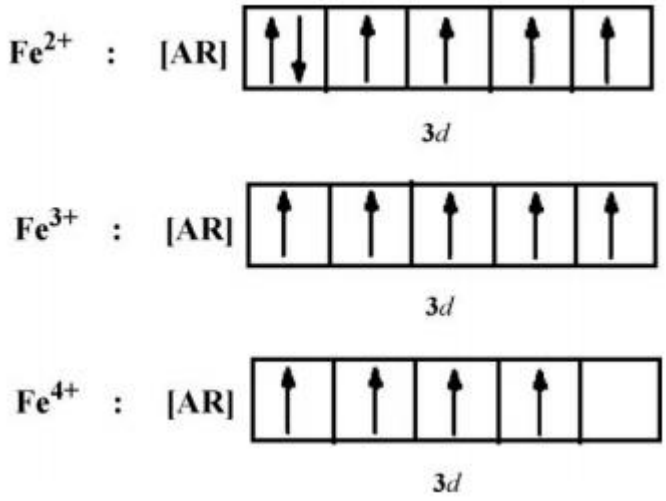

Figure 2.4: The electron configuration of Fe^{2+}, Fe^{3+} and Fe^{4+} (Yu, Xiang and Zhou, 2009).

2.5 Sonophotocatalytic Activities of ZnO towards Phenol Degradation

ZnO-based catalysts have has been used widely in degradation varieties of phenolic compounds and achieved high efficiency of degradation. According to the experiments conducted by Qin et al (2017), the sonophotcatalytic degradation of 4-nitrophenol presence of 1.4 g/L ZnO micro-nanoparticles under 300 w UV Hg lamps. Their results showed an excellent degradation of 4-nitrophenol and achieved 90.5% degradation efficiency after 120 min irradiation. Lavand and Malghe (2015) also using C/ZnO/CdS as catalysts demonstrated a high egradation of 98% under sonophotocatalytic experiments. The data of sonophotocatalytic activities of ZnO on different type of phenols degradation are shown in Table 2.1.

Table 2.1: Sonophotocatalytic Activity of ZnO on Phenolic Compound Pollutants

Sonophotocatalyst	**Target compound**	**Reaction Condition**	**Degradation Efficiency (%)**	**References**
C/ZnO/CdS	4-Chlorophenol	Under 65 W compact fluorescent lamp irradiation; 4-CP concentration = 10 ppm; volume = 100 mL; catalyst loading = 0.05 g; irradiation time = 120 min	98	Lavand and Malghe (2015)
ZnO MNPs	4-Nitrophenol	Under 300 W UV Hg lamp irradiation; volume = 20 mL; catalyst loading = 1.4 g/L; solution pH = 8; irradiation time = 120 min	90.5	Qin et al (2017)
ZnO	Phenol	Under 400 W UV lamp irradiation; under 100 W US output power at 40 KHz; volume = 100 mL; catalyst loading = 0.1 g; solution pH = 5.5; irradiation time = 2 h	85	Anju, Yesodharan and Yesodharan (2012)

TiO_2-ZnO	Phenol	Under 40 W UV bulb irradiation; under 300 W US output power at 35 KHz; phenol concentration = 10 mg/L; volume = 500 mL; catalyst loading = 0.25 g; irradiation time = 1 h	99.31	Fatimah and Novitasari (2016)
ZnO	Phenol	Under 400 W UV lamp irradiation; under 100 W US output power at 40 KHz; phenol concentration = 40 mg/L; catalyst loading = 140 mg/L; solution pH = 5.5; irradiation time = 2 h	90	Jyothi, Yesodharan and Yesodharan (2014)
ZnO	Salycilic Acid	Under 20 W UV Lamp of Philips; under 300 W US output power at 35 KHz; volume = 500 mL; catalyst loading = 0.2 g; irradiation time = 120 min	-	Fatimah et al (2017)

2.6 Effects of Operating Parameters

2.6.1 Effect of Initial Substrate Concentration on the Sonophotocatalytic Degradation of Phenolic Compounds

The effect of initial concentration of the phenolic compound is an important aspect that can affect the process performance (Ye et al., 2015). Several researches have shown that the degradation efficiency decreased when the initial concentration of phenolic compound increased (Ye et al., 2015; Dewidar, Nosier and El-Shazly, 2017).

The relationship between phenolic compound concentration and degradation efficiency can be explained by the competence between •OH ion and $\bullet O_2^-$ radical adsorption on the catalyst surface (Selvam et al., 2013). The phenolic compound molecules are being oxidised by catalyst's active sites or hydroxyl radicals (•OH) that generated on catalyst's surface. The photo-generated electron-hole pairs are generated to undergo redox reactions to produce •OH and $\bullet O_2^-$ radicals for organic pollutants degradation (Ashar et al., 2016).

Increment in phenolic compound concentration can reduce the generation of •OH radicals due to the adsorption of phenolic compound on the active sites of catalyst. Furthermore, the availability of active sites for generation of •OH radicals and degradation rate decreased with fixed irradiation time and amount of catalyst (Dewidar, Nosier and El-Shazly, 2017). Instead of sonophotocatalyst, generated photons can be absorbed by phenolic compound, causing lesser photons to reach the catalyst surface. Hence, it will caused the generation of •OH radicals decreased. Moreover, intermediates may be formed in the process of sonophotodegradation of phenol. The intermediates on catalyst surface can cause the deactivation of active sites. (Selvam et al.,2013; Ashar et al., 2016).

The experiments conducted by Ye et al (2015) showed the 4-chlorophenol (4-CP) photocatalytic degradation over ZnO nano-particles was affected by initial concentration of 4-CP. The results showed a significant drop of degradation efficiency from 99.5% to 74.2% when the 4-CP concentration increased from 50

mg/L to 200 mg/L. Table 2.2 was tabulated the other examples of researches on effect of initial phenolic compound concentration over ZnO photocatalyst.

Table 2.2: Effect of Initial Substrate Concentration on the Sonophotocatalytic Degradation of Phenolic Compounds

Phenolic Compound	**Sonophotocatalyst**	**Tested Initial Phenolic Compound Concentration**	**Maximum Degradation Efficiency on Tested Initial Phenolic Compound Concentration (%)**	**References**
Phenol	ZnO	25 – 100 ppm	78.2 (25 ppm)	Dewidar, Nosier and El-Shazly (2017)
Nonylphenol ethoxylate	ZnO flower and pseudo-sphere	50 - 150 mg/L	95 (50 mg/L)	Ashar et al (2016)
Phenol	ZnO nanosheets immobilised	10 - 60 mg/L	88.5 (10 mg/L)	Ye et al (2015)
4-Chlorophenol	Pt@BiOI/ZnO	20 – 50 mg/L	99.9 (25 mg/L)	Jiang et al (2018)
2-Chlorophenol	ZnO-ZnS@polyaniline nanohybrid	25 – 10 mg/L	88 (25 mg/L)	Anjum et al (2017)

2.6.2 Effect of Solution pH

Industrial wastewater can be discharged a various pH values, as it can affect the photocatalytic degradation efficiency (Lee et al., 2016). Solution pH affects the surface charge of the catalyst particles, as well as the positions of conduction and valence bands in ZnO (Haque et al., 2006). The change in quantity and way of adsorption of organic pollutants on the surface of ZnO can bring significant changes to the photocatalytic degradation efficiency (Hassan, 2011).

The effect of solution pH can be explained on the basis of Zero Point Charge (pH_{ZPC}). Zero Point Charge is defined as the pH at which the surface of a catalyst is uncharged. The pH_{ZPC} of ZnO was estimated to be 9.3 (Hassan, 2011). In aqueous solution with pH higher than its pHzpc, ZnO surface was negatively charged by adsorbed OH^- ions. The reactions are shown in the following Equations 2.21 – 2.22 (Lam et al., 2012).

$$ZnOH + H^+ \leftrightarrow ZnOH_2^+ \quad (2.21)$$

$$ZnOH + OH^- \leftrightarrow ZnO^- \quad (2.22)$$

Moreover, solution pH can transform the interaction and affinity between the photocatalyst surface and phenolic molecules due to each phenolic compound has its own nature. Molecular form of phenolic compound can form strong electrostatic attraction with ZnO in an acidic solution as ZnO was protonated at low pH. This can promote the adsorption of phenolic compound on ZnO surface and led to a rise in degradation efficiency of ZnO (Dewidar, Nosier and El-Shazly, 2017). However, the degradation efficiency can be hampered when both the phenolic molecules and ZnO photocatalyst have the same charge. It should be noted that, the degradation efficiency of ZnO can also be enhanced at high pH as the large amount of OH^- ions adsorbed on ZnO surface that favoured formation of hydroxyl radical (·OH) radicals for degrading the phenolic molecules. Thus, the multiple roles of solution pH on the photocatalytic degradation process should be carried out carefully to optimise the efficiency of a reaction (Anjum et al., 2017).

Referring to the study on photocatalytic degradation of phenol by ZnO carried out by Pardeshi and Patil (2008), the effect of solution pH towards ZnO's degradation efficiency was clearly seen. From the result, ZnO exhibited the highest efficiency at pH of 5.61. According to a simple surface charge model, phenol was anionic compound having negative charges which adsorbed easily on the ZnO surfaces in case of solution pH that below pHpzc. On the other hand, phenol anions would be repelled from the negatively charged ZnO photocatalyst surface at pH above the pHpzc.

Furthermore, Ashar et al (2016) also reported on the effect of solution pH on degradation efficiency of nonylphenol ethoxylate using ZnO flower and pseudo-sphere. The results obtained showed that C-doped ZnO achieved 95% of degradation efficiency at pH 6. Other than less amount of OH^- ions were adsorbed on the ZnO surface at low pH, dissolution of ZnO may also took place, which decreased the degradation efficiency. Table 2.3 was recorded the other examples of researches on effect of solution pH over ZnO photocatalyst.

Table 2.3: Effect of Solution pH on the Sonophotocatalytic Degradation of Phenolic Compounds

Phenolic Compound	**Sonophotocatalyst**	**Range of Solution pH Tested**	**Optimum Solution pH**	**Degradation Efficiency (%)**	**References**
Phenol	ZnO	3 - 11	5.61	47	Pardeshi and Patil (2008)
2-Phenylphenol	ZnO	6.6 - 12	6.6	99	Khodja et al (2001)
2,4-Dichlorophenol	ZnO	3 - 11	5.9	72.2	Sin et al (2013)
Phenol	Ag/ZnO	2 - 8	6.5	88	Vaiano et al (2018)
Nonylphenol ethoxylate	Pt@BiOI/ZnO	4 - 10	6	95	Ashar et al (2016)
Phenol	ZnO nanosheets immobilised	5 - 9	6.97	80.9	Ye et al (2015)

2.6.3 Effects of Catalyst Loading

Generally, increase in photocatalyst loading can increase the photocatalytic degradation efficiency. This is related to the effective surface area of catalyst and the absorption of light (Sin et al., 2012). As photocatalyst loading increased, the available active sites on the photocatalyst surface increased, allowing more number of photons to be absorbed to generate more •OH radicals. This can lead to a higher degradation efficiency of ZnO (Sin, Lam and Mohamed, 2010).

Furthermore, when the amount of ZnO is overloaded, the turbidity of the solution increased, causing light scattering effect and limited UV light penetration, subsequently led to a reduction of number of active sites on ZnO surface (Sin et al., 2012; Kaur, Bansal and Singhal, 2013). This resulted in the shrinking of the effective photoactivated volume of suspension (Sin et al., 2012). Besides, overloading of photocatalyst can lead to particle aggregation, causing reduction of effective surface area as it does not increase in geometrical ratio. Hence, an optimum amount of photocatalyst loading has to be determined (Wang et al., 2007).

Casillas et al., 2017 studied the effect of Al-Nd-Zn photocatalysts dosage (0.8 – 2.0 wt %) on the photocatalytic degradation efficiency of phenol. The photocatalytic degradation efficiency of phenol increased drastically from 0.25-1.5 g/L, however relatively small increment was shown afterwards. The reported optimum loading of ZnO was 1.2 wt%, which achieved maximum degradation efficiency. According to Modirshahla et al. 2011, the degradation efficiency of ZnO increased with the increasing amount of loading from 150 to 900 mg/L. The efficiency of ZnO dropped, from 99.9% to 80%, as the amount of loading further increased to 1050 mg/L. Table 2.4 was tabulated the other examples of researches on effect of catalyst loading over ZnO photocatalyst.

Table 2.4: Effect of Catalyst Loading on the Sonophotocatalytic Degradation of Phenolic Compounds

Phenolic Compound	**Sonophotocatalyst**	**Tested Catalyst Concentration (g/L)**	**Optimum Catalyst Concentration (g/L)**	**Degradation Efficiency (%)**	**References**
Phenol	ZnO	0.2 – 0.8	0.6	88	Parida and Parija (2006)
Estrone	ZnO	0.01 – 1.00	0.5	95	Han et al (2012)
Lignin	TiO_2/ZnO	0.5 – 2.0	1.0	98	Kansal, Singh and Sud (2008)
4-Chlorophenol	ZnO	0.5 – 3.0	2.0	96	Gaya et al (2009)
4-Nitrophenol	ZnO/nanoclinoptilolite zeolite	0.25 – 5.00	1.5	90	Nezamzadeh-Ejhieh and Khorsandi (2014)

CHAPTER 3

METHODOLOGY

3.1 Overall Flow Chart of the Work

Several experimental steps were carried out in this study, which have been summarised in the Figure 3.1.

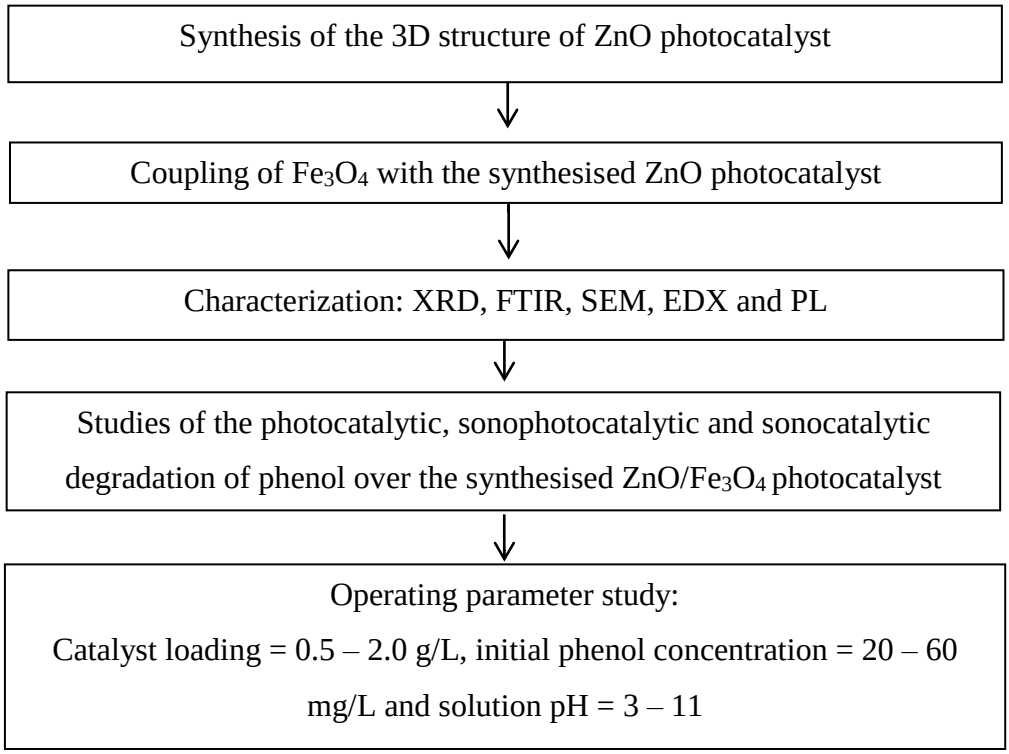

Figure 3.1: Flow Chart of the Overall Methodology

3.2 Materials and Chemicals

The materials and chemicals used in the experiment are listed in Table 3.1.

Table 3.1: List of Chemicals and Materials Used

Chemical / Material	Purity	Supplier	Application
Distilled Water		Gainson Advanced Technology	Preparation of phenol solution and photocatalyst synthesis
Sodium Hydroxide (NaOH)	≥ 96%	Uni-Chem Reagents	Photocatalyst synthesis
Zinc (II) Nitrate Hexahydrate ($Zn(NO_3)_2 \cdot 6H_2O$)	98%	Sigma-Alrich	Zinc precursor
Iron (II, III) Oxide (Fe_3O_4)	97%	Alfa Aesar	Coupled semiconductor
Sulfuric Acid (H_2SO_4)	97%	QReC	pH adjustment

3.3 Catalyst Preparation

In this research, zinc (II) nitrate hexahydrate was used as the precursor through chemical precipitation method to produce hierarchical ZnO structures. 4 mmol of zinc (II) nitrate hexahydrate ($Zn(NO_3)_2•6H_2O$) was dissolved into 80 mL of distilled water under stirring. Next, 24 mmol of NaOH was added into the mixture. After 3 hours of stirring, the white precipitation was collected, filtered and washed with distilled water for 3 times. Subsequently, the samples were dried at 65 ˚C in an oven for 17 hours.

For the ZnO/Fe_3O_4 photocatalysts preparation 1 g of ZnO powders were mixed with different weight percentages of Fe_3O_4 (1 – 9 wt%). 100 mL of distilled water was added into the mixture and placed in ultrasonic bath for 30 minutes. Then, a magnetic stirrer was used to stir the mixture for 20 hours and dried at 65 ˚C in an oven for 17 hours. The dried mixtures were grinded into fine powders, and followed by calcined at 450 ˚C for 2 hours. Figure 3.2 shows procedures for synthesizing the three-dimensional ZnO/Fe_3O_4 photocatalysts.

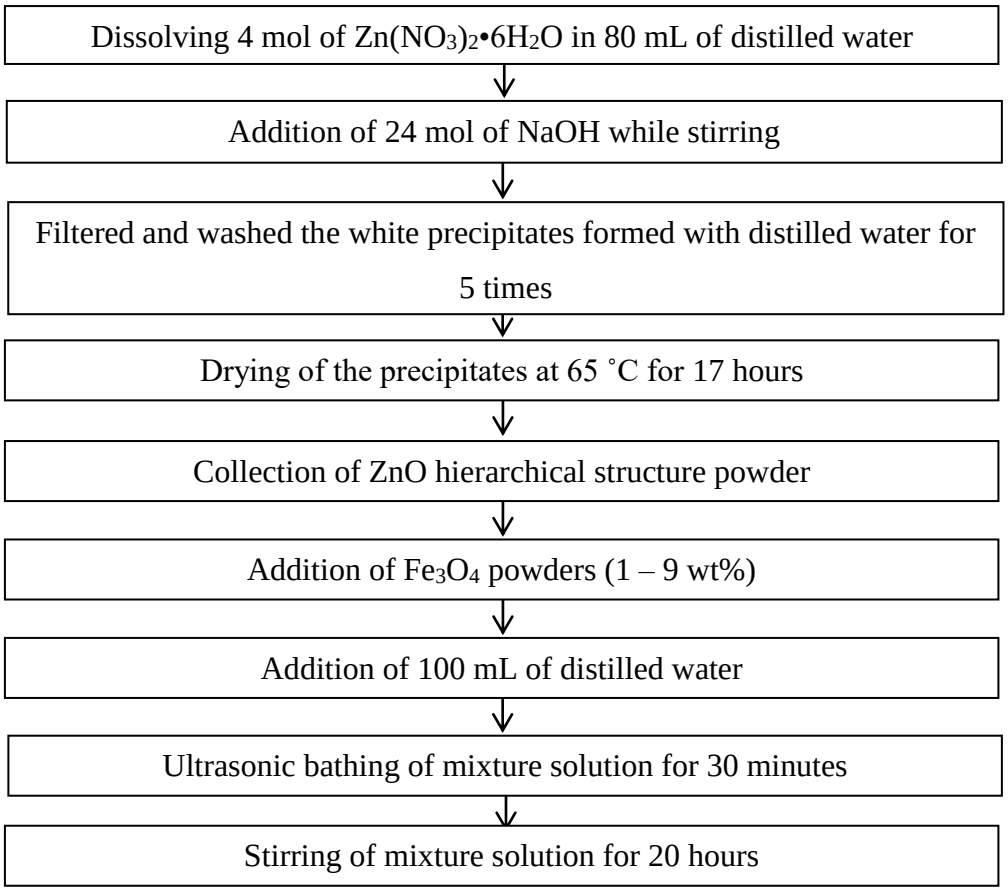

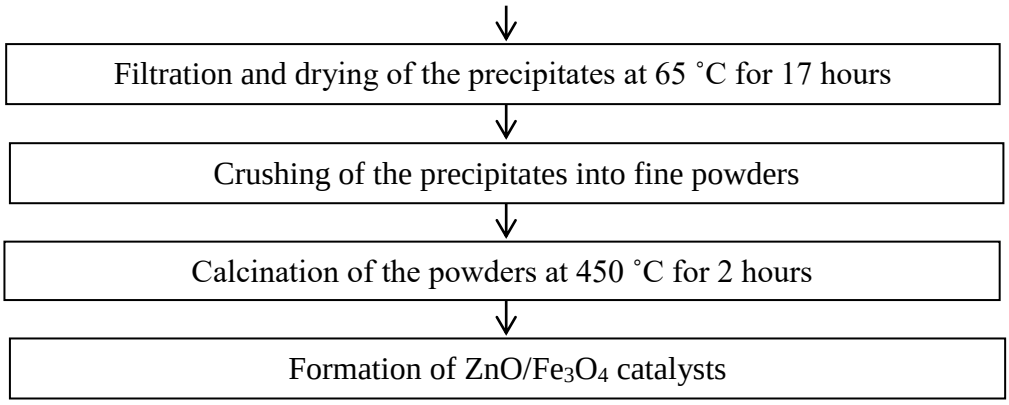

Figure 3.2: Flow Chart of Synthesis Process of Three-Dimensional ZnO/Fe_3O_4 Catalysts

3.4 Characterisation Study

3.4.1 X-ray Diffraction (XRD)

The crystal phase of ZnO/Fe_3O_4 photocatalysts was analysed by X-ray diffraction (XRD), which scanned at 2θ from 20˚ to 90˚. The machine used was XRD-6000 supplied by Shimadzu. This study was conducted at the Faculty of Science, UTAR.

3.4.2 Scanning Electron Microscopy (SEM) and Energy Dispersive X-ray (EDX) Spectroscopy

Scanning electron microscope was use to analyse the surface morphology of ZnO/Fe_3O_4 photocatalysts, with JSM 6701-f supplied by Jeol, Japan. For the analysis, photocatalysts powder was placed evenly on a double sided carbon tape and attached onto an aluminium stub. Different magnifications were used to scan the sample of ZnO powder. Besides, determination of the sample's elemental composition was conducted by energy dispersion X-ray (EDX), via the Oxford Instrument 50 mm^2 supplied from England. This study was conducted at the Faculty of Science, UTAR.

3.4.3 Fourier Transform Infrared (FTIR) Spectroscopy

Fourier Transform Infrared Spectroscopy (FTIR) was used to analyse the functional group of photocatalysts composite with Spectrum Ex 1 machine model supplied by Perkin Elmer. The catalyst was grinded into fine powder with potassium iodide (KI), with the ratio of 1:10. The powders were then flattened at high pressure with duration of 15 seconds to form a thin film to be used for the analysis. This study was conducted at the Faculty of Science, UTAR.

3.4.4 Photoluminescence (PL) Spectroscopy

PL spectroscopy provided the information on the electronic structure of catalysts. The PL spectroscopy of as-synthesised catalysts was taken at room temperature on a spectrofluorometer (model: Perkin Elmer Lambda S55) in the range of 400 nm and 550 nm. The 325 nm emission of a Xe lamp was used for exciting the catalysts. The study was conducted at School of Chemical Engineering, Universiti Sains Malaysia.

3.5 Experiment Setup

3.5.1 Photocatalytic, Sonocatalytic and Sonophotocatalytic Degradation

The laboratory experiment set up consisted of a batch reaction system. Figure 3.3 (a) and (b) illustrates the schematic diagram and laboratory setup for the photocatalytic degradation. The photocatalytic degradation experiments were demonstrated in a volume of 250 mL beaker. A 105 W fluorescent lamp was used as the light source for irradiation during the process of degradation which place above the phenol solution. A hot plate stirrer (model: Fisher Scientific) was used to stir the mixture to ensure homogeneous mixing was achieved. An acrylic black box with the purpose of blocking stray light, was used to cover the beaker, lamp and hotplate stirrer throughout the entire experiment. An air pump (model: Sobo) was used to supply oxygen to the photocatalyst in phenol solution for the experiment. In addition, the amount of air entering the system was controlled by a flow meter (model: Dwyer). Cooling blower fans (model: Toyo) was installed to reduce the temperature and cooling purpose.

Moreover, Figure 3.4 (a) and (b) illustrates the schematic diagram and laboratory setup for the sonophotocatalytic degradation. The sonophotocatalytic degradation experiments were demonstrated in a volume of 250 mL beaker. A 105 W fluorescent lamp was used as the light source for irradiation during the process of degradation which place above the phenol solution. A 100 W power output with 40 KHz ultrasonic water bath (model: Elmasonic) with 40 KHz was used to ensure the mixture achieved homogeneous mixing. An acrylic black box with the purpose of blocking stray light, was used to cover the beaker, lamp and ultrasonic water bath throughout the entire experiment. An air pump (model: Sobo) was used to supply oxygen to the photocatalyst in phenol solution throughout the experiment. In addition, the amount of air entering the system was controlled by a flow meter (model: Dwyer). Cooling blower fans (model: Toyo) was installed for reduce temperature and cooling purpose.

Next, Figure 3.5 (a) and (b) illustrates the schematic diagram and laboratory setup for sonocatalytic degradation. The sonocatalytic degradation experiments were demonstrated in a volume of 250 mL beaker. A 36 W fluorescent lamp was used as the light source for irradiation during the process of degradation which place above the phenol solution. A 100 W power output with 40 KHz ultrasonic water bath (model: Elmasonic) was used to ensure the mixture achieved homogeneous mixing. An air pump (model: Sobo) was used to supply oxygen to the photocatalyst in phenol solution for the experiment. In addition, the amount of air entering the system was controlled by a flow meter (model: Dwyer).

(a) (b)

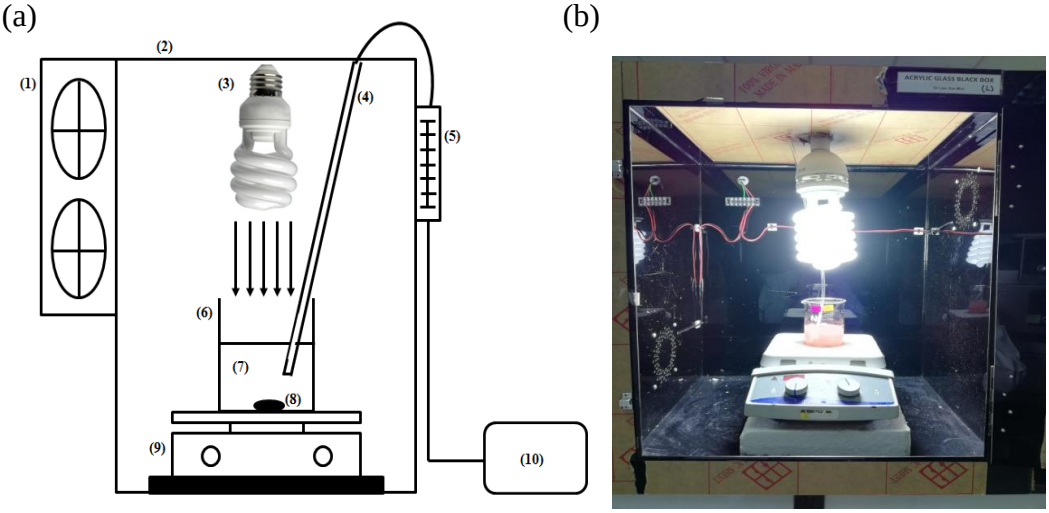

Figure 3.3: Photocatalytic Degradation Reaction System under Fluorescent Light Irradiation (a) Schematic Diagram and (b) Laboratory Setup

(1) Cooling Blower Fans, (2) Acrylic Black Box, (3) Fluorescent Lamp, (4) Air Supply, (5) Flow Meter, (6) Beaker, (7) Phenol Solution, (8) Magnetic Bar, (9) Hot Plate Stirrer and (10) Air Pump.

(a) (b)

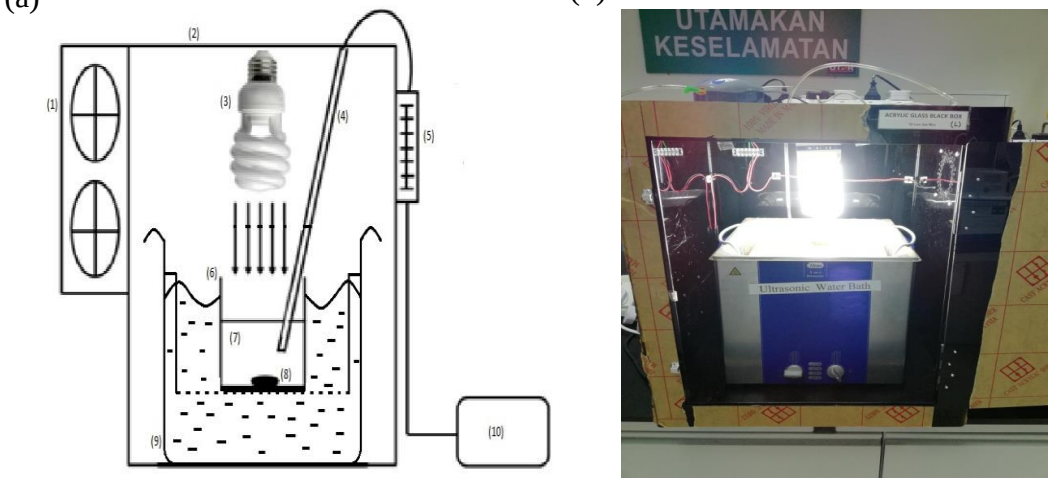

Figure 3.4: Sonophotocatalytic Degradation Reaction System under Fluorescent Light Irradiation and Ultrasonic Water Bath (a) Schematic Diagram and (b) Laboratory Setup

(1) Cooling Blower Fans, (2) Acrylic Black Box, (3) Fluorescent Lamp, (4) Air Supply, (5) Flow Meter, (6) Beaker, (7) Phenol Solution, (8) Magnetic Bar, (9) Ultrasonic Water Bath and (10) Air Pump.

(a) (b)

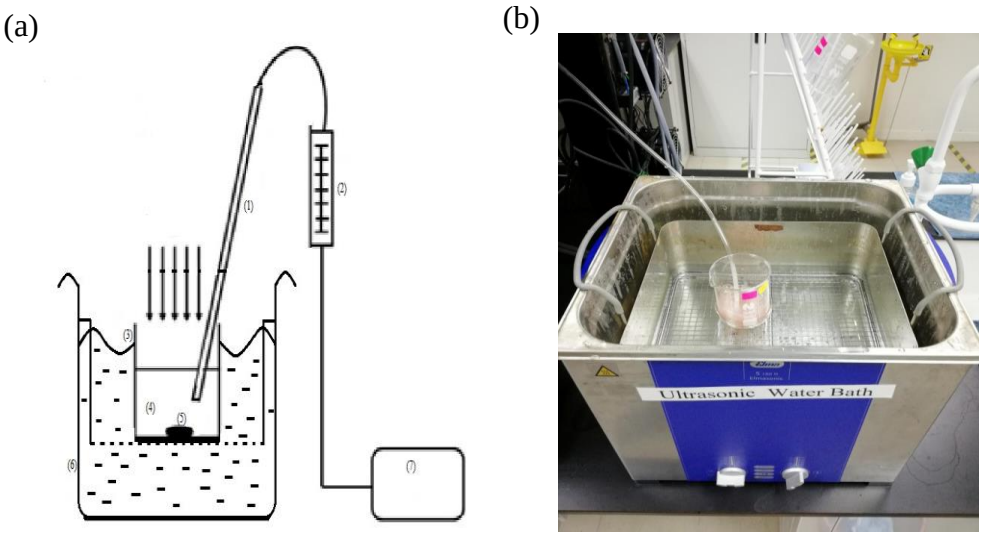

Figure 3.5: Sonocatalytic Degradation Reaction System in Ultrasonic Water Bath (a) Schematic Diagram and (b) Laboratory Setup

(1) Air Supply, (2) Flow Meter, (3) Beaker, (4) Phenol Solution, (5) Magnetic Bar, (6) Ultrasonic Water Bath and (7) Air Pump.

3.6 Catalytic Degradation Performance

In this study, phenol was applied to study the performance of ZnO/Fe_3O_4 in the photocatalysis, sonophotocatalysis and sonocatalysis reactions. The catalytic degradation was demonstrated in a batch reaction system with developed nanocomposite photocatalyst under a 105 W fluorescent lamp irradiation. At first, 100 mL of phenol solution with 1.5 g/L of ZnO/Fe_3O_4 loading were prepared and added into a beaker for photocatalysis and sonophotocatalysis. On the other hand, 100 mL of phenol solution with 1.0 g/L of ZnO/Fe_3O_4 loading was prepared for sonocatalysis. Then, constant air flow at 6 mL/min was bubbled into the solution mixture throughout the entire experiment for all runs. Before starting the reactions, the mixture prepared was premixed in the dark for 30 minutes to prevent exposing it to light irradiation to achieve the equilibrium adsorption-desorption of pollutant on catalyst surface. After the dark run process, sonophotocatalysis and sonocatalysis mixtures will be moved into ultrasonic water bath for the reaction performance. While, photocatalysis mixtures will be stirred continuously by a hot plate stirrer to ensure homogeneous mixing. For every 30 minutes, 4 mL of sample solution was collected from the mixture solution. The sample solution was collected and filtered by 0.45 μm PTFE syringe fillers and analysed by High Performance Liquid Chromatography (HPLC). The phenol degradation efficiency was calculated using the formula shown in Equation 3.1:

$$\text{Phenol degradation efficiency (\%)} = \frac{C_0 - C_t}{C_0} \times 100\% \qquad (3.1)$$

Where,

C_0 = Concentration of phenol after 30 min run in dark

C_t = Concentration of phenol after reaction time, t (min)

3.7 Effect of Operating Parameters

3.7.1 Effect of Initial Phenol Concentration

The effect of initial phenol concentration on the catalytic phenol degradation was studied by performing the experiments with varying initial phenol concentration ranging from 20 to 60 mg/L over the synthesised ZnO/Fe_3O_4 composites. Photocatalytic and sonophotocatalytic degradation experiment runs were performed with a fixed 1.5 g/L catalyst loading and solution pH of 5. While, sonocatalytic degradation experiment runs with a fixed 1.0 g/L catalyst loading and a solution pH of 5.

3.7.2 Effect of Solution pH

The effect of solution pH on the catalytic degradation of phenol was carried out by performing the experiments with varying solution pH ranging from 3 to 11 over the synthesised ZnO/Fe_3O_4 composites. The solution pH was adjusted by adding either 0.1M of H_2SO_4 or NaOH solution before starting the experiment. The pH adjustors were prepared by diluting the corresponding acid and alkaline with distilled water. The different solution pH values were selected depending on the conditions such as acidic, natural, neutral and alkaline. Photocatalytic and sonophotocatalytic degradation experiment were performed with 20 mg/L initial phenol concentration and 1.5 g/L catalyst loading. While, sonocatalytic degradation experiment runs with 20 mg/L initial phenol concentration and fixed 1.0 g/L catalyst loading.

3.7.3 Effect of Catalyst Loading

The effect of catalyst loading on the catalytic degradation of phenol was carried out by performing the experiments with varying catalyst loading ranging from 0.5 to 2.0 g/L over the synthesised ZnO/Fe_3O_4 composites. Catalyst loading can be fixed by manipulating the catalyst amount that fed into the reactor. All the experiments were performed with a fixed 20 mg/L initial phenol concentration and a solution pH of 5.

CHAPTER 4

RESULTS AND DISCUSSIONS

4.1 Characterisation

Characterisation analyses were conducted on ZnO, Fe_3O_4 and ZnO/Fe_3O_4 in order to determine their structures and functional groups. The analyses carried out were X-ray diffraction (XRD), fourier transform infrared (FTIR) spectroscopy, scanning electron microscopy (SEM), energy dispersive X-ray (EDX) spectroscopy and photoluminescence (PL) spectroscopy.

4.1.1 X-ray Diffraction (XRD)

XRD was applied to analyse the phase structure and crystallinity of the synthesised ZnO, Fe_3O_4 and ZnO/Fe_3O_4 samples, various results are shown in Figure 4.1 (a), (b) and (c). The peaks in the XRD pattern were very sharp and intense which showed that the samples were good crystalline in nature. Figure 4.1 (c) shows diffraction peaks of ZnO at 2θ values 34.46◦, 37.08◦, 38.94◦ 50.26◦, 59.34◦, 65.60◦, 69.08◦, 70.68◦, 71.84◦, 75.30◦ and 79.78◦ with corresponding diffraction planes of (100), (002), (101), (102), (110), (103), (200), (112), (201), (004) and (002) respectively. Figure 4.1 (b) shows diffraction peaks of Fe_3O_4 at 2θ values 29.88◦, 34.70◦, 45.86◦ 53.80◦, 59.78◦, 65.38◦, 73.72◦ and 76.86◦ with corresponding diffraction planes of (220), (311), (400), (422), (511), (402), (620) and (533) respectively. Figure 4.1 (a) shows diffraction peaks of ZnO/Fe_3O_4 nanocomposites at 2θ values 34.26◦, 45.86◦,

53.28◦ 59.78◦ and 65.38◦ with corresponding diffraction planes of (311), (400), (422), (511) and (402) respectively. The diffraction peaks for ZnO/Fe_3O_4 nanocomposites spectrum were in complete agreement in the peak position and relative intensity as compared to ZnO nanoparticles.

The diffraction peaks of ZnO were corresponded to hexagonal wurtzite crystalline structure (Vinod et al., 2015). The Zn atom of wurtzite ZnO crystalline structure was coordinated with four oxygen atom. Each oxygen atom binds with four Zn atoms in tetrahedral ZnO. Hence, hexagonal wurtzite ZnO has two independent polar faces which are Zn^{2+} face and O^{2-} ions face (Hitkari, Singh and Pandey, 2017). From the results, ZnO crystal structure can be remained unchanged in the ZnO/Fe_3O_4 nanocomposites as ZnO nanoparticles were in situ formed. On the other hand, the diffraction peaks of Fe_3O_4 were corresponded to inverse cubic spinel structure as the crystalline structure of Fe_3O_4 can be remained after coupling with ZnO (Wei et al., 2012). The diffraction peaks of ZnO/Fe_3O_4 nanocomposites decreases as compared to ZnO nanoparticles due to ZnO has lower molar ratio than Fe_3O_4 in ZnO/Fe_3O_4 nanocomposites (Abazari, Mahjoub and Sanati, 2016). Hence, it shows that the ZnO/Fe_3O_4 composites are completely synthesised by ZnO and Fe_3O_4 as there are no other diffraction peaks were reported. A similar results of diffraction peaks has been reported from other literatures (Abazari, Mahjoub and Sanati, 2016; Bustos-Torres et al., 2017; Hitkari, Singh and Pandey, 2017; Gharagozlou and Naghibi, 2018; Hao et al., 2018; Kumar et al., 2018).

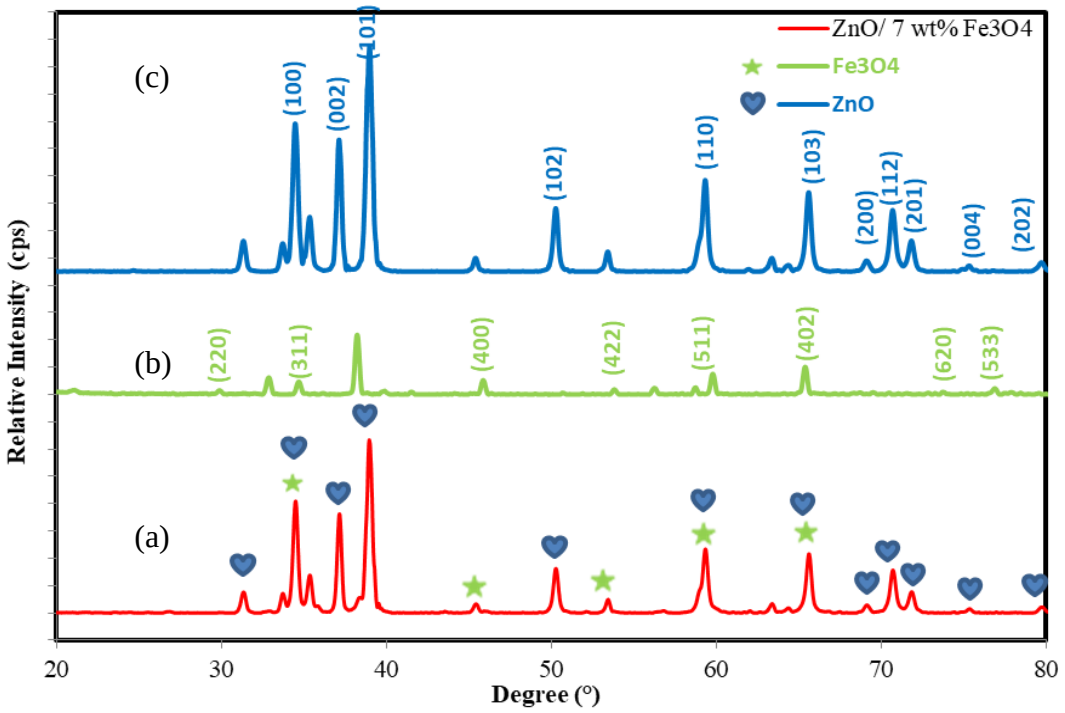

Figure 4.1: XRD Spectrum of Synthesised ZnO, Fe_3O_4 and ZnO/ 7 wt% Fe_3O_4 Catalysts

4.1.2 Fourier Transform Infrared (FTIR) Spectroscopy

FTIR characterisation can detect to the vibrations of metal–oxygen bonds that the regions lower than 1000 cm^{-1}. Hence, the formation of the metal oxide can be ensured by the regions (Abazari, Mahjoub and Sanati, 2016). Besides, it revealed crucial information for the functional groups and analytical tool for measuring compound purity on the surface of the synthesised photocatalysts (Shivaramu et al., 2017). Figure 4.2 shows the FTIR analysis of ZnO, Fe_3O_4, and ZnO/ Fe_3O_4 composite in the range of 400 – 4,000 cm^{-1}.

There were three important peaks in the ZnO spectrum at 560, 1540, and 3432 cm^{-1}, which are the Zn–O, C–O, and –OH stretching vibrations. The absorption peak at 1637 cm^{-1} and 3432 cm^{-1} related to the O-H stretching vibrations of surface adsorbed moisture (Yang et al., 2010; Shivaramu et al., 2017). The results of ZnO/Fe_3O_4 spectrum shows that the main peaks of ZnO and Fe_3O_4 are 427 cm^{-1} and 570 cm^{-1}. This proved the existence of ZnO and Fe_3O_4 in the as–prepared sample. Both overlapping of Zn-O and Fe-O stretching were caused the formation of 570 cm^{-1} peak (Gharagozlou and Naghibi, 2018). According to the FTIR results, ZnO/Fe_3O_4 consist a very similar pattern with the spectra of both ZnO and Fe_3O_4 molecules that indicates hybridisation of ZnO and Fe_3O_4. Hence, it can be known that the photocatalyst consist of the functional groups of Zn-O and Fe-O. A similar results has been reported from other literatures (Yang et al., 2010; Abazari, Mahjoub and Sanati, 2016; Bustos-Torres et al., 2017; Shivaramu et al., 2017; Kumar et al., 2018).

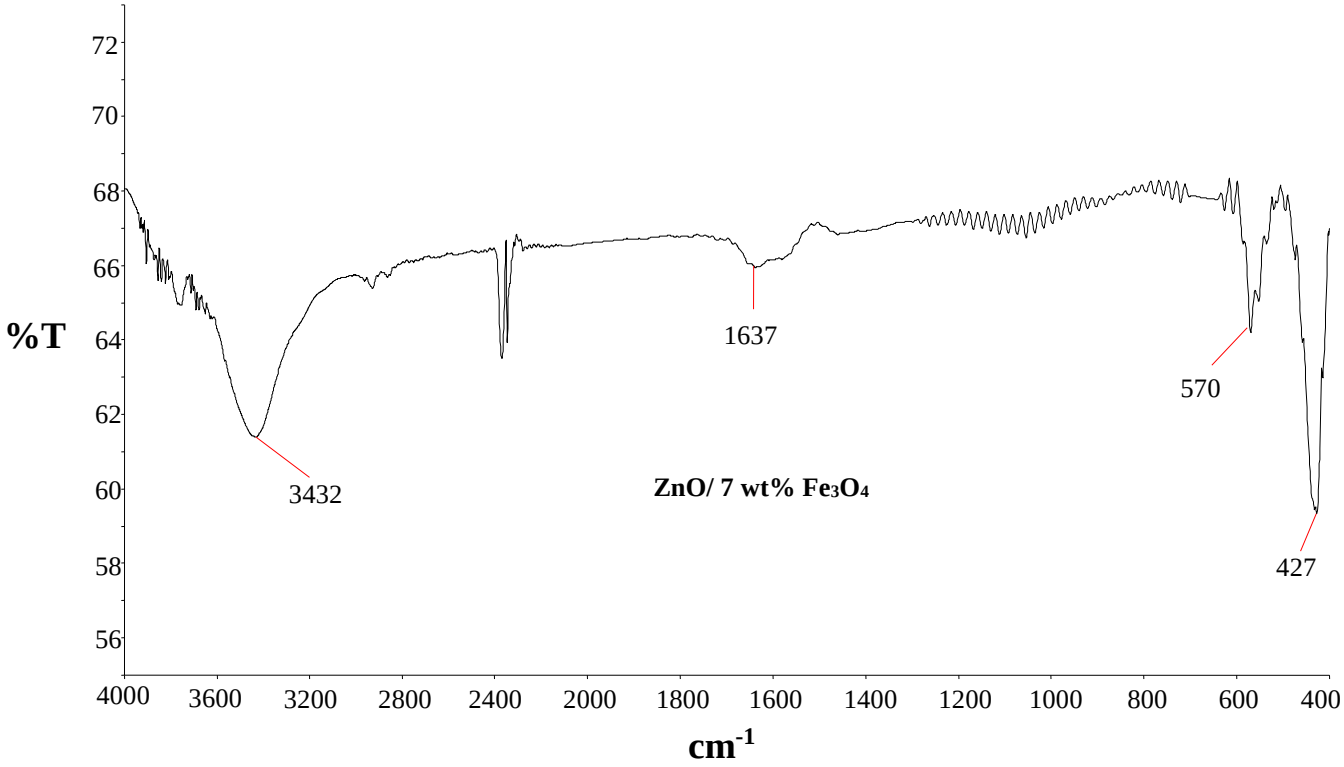

Figure 4.2: FTIR Spectra of ZnO/ 7 wt% Fe_3O_4

4.1.3 Scanning Electron Microscopy (SEM) and Energy Dispersive X-ray (EDX) Spectroscopy

The scanning electron microscopy images of ZnO, Fe_3O_4 and ZnO/Fe_3O_4 photocatalysts shows in Figure 4.3 (a), (b) and (c). The SEM images were demonstrated to reveal the surface morphology and the phase distribution of synthesised ZnO/Fe_3O_4 nano-composites. From the images, ZnO composites formed three dimensional hierarchical structures in spherical shapes and the Fe_3O_4 particles were strongly deposited on the ZnO composites surface. The EDX analyses shows in Figure 4.3 (d), (e) and (f). The EDX spectrum of ZnO, Fe_3O_4 and ZnO/Fe_3O_4O has confirmed the presence of Zn, O, and Fe elements. These indicated a good hybridisation between ZnO and Fe_3O_4 composites and confirm that the synthesised photocatalysts are ZnO/Fe_3O_4.

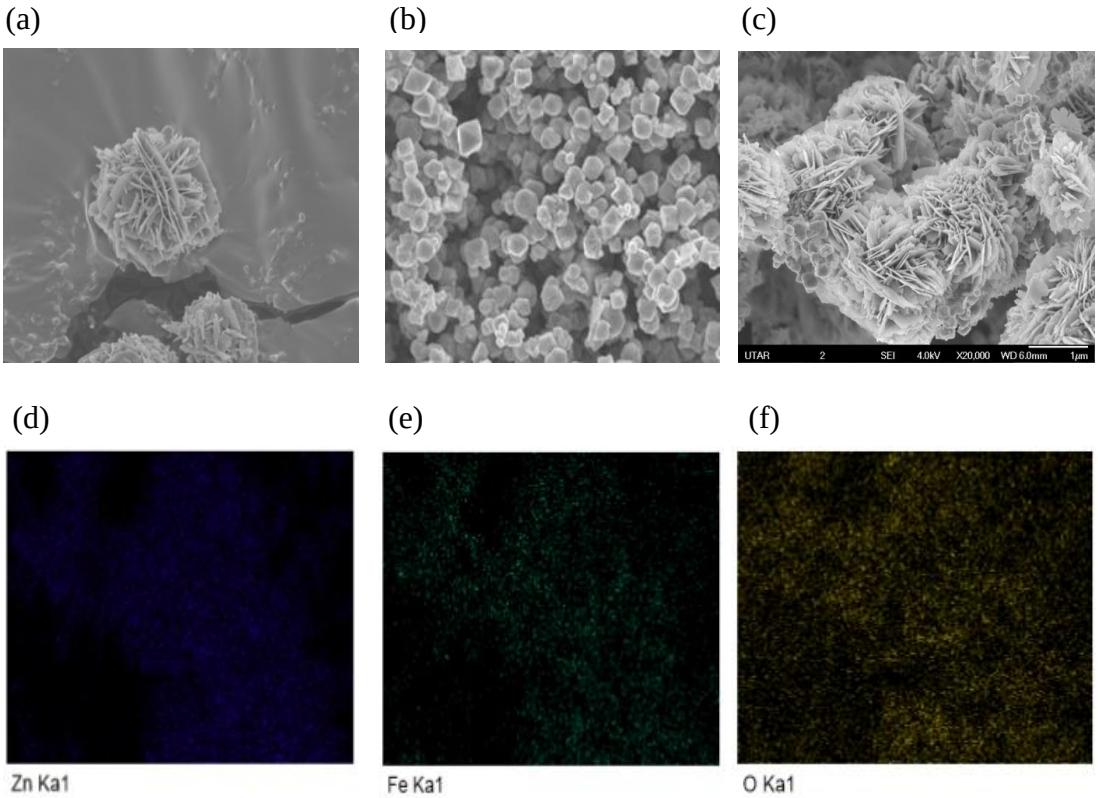

Figure 4.3: SEM Images (×20,000 Magnifications) of (a) ZnO, (b) Fe_3O_4 and (c) ZnO/Fe_3O_4 EDX Images of Catalysts Elements (d) Zn, (e) Fe and (f) O

4.1.4 Photoluminescence (PL) Spectroscopy

The PL characterisations of the as-synthesised photocatalysts were recorded to examine the potential, optical and electronic applications. The photogenerated electron–hole pair recombination rates were evaluated by the PL excitation spectra. Figure 4.4 shows the results of ZnO, ZnO/ 1 wt% Fe_3O_4, ZnO/ 3 wt% Fe_3O_4, ZnO/ 5 wt% Fe_3O_4, ZnO/ 7 wt% Fe_3O_4 and ZnO/ 9 wt% Fe_3O_4 samples. PL spectrum with low intensity showed that more electrons and holes participate in the oxidation and reduction reactions due to the enhanced separation of the charge carriers (Shekofteh-Gohari and Habibi-Yangjeh, 2017). From the Figure 4.4, similar spectra at around 475 – 500 nm can be seen from the samples. The peaks around 425 nm can be recombined of free excitons (Pandiyarajan, Baesso and Karthikeyan, 2014). While, the peaks around 480 nm could be originated from defect state luminescence (Raj and Sadayandi, 2016).

From the results, the emission intensity of the ZnO/ 1 wt% Fe_3O_4, ZnO/ 3 wt% Fe_3O_4, ZnO/ 5 wt% Fe_3O_4, ZnO/ 7 wt% Fe_3O_4 and ZnO/ 9 wt% Fe_3O_4 samples are slightly lower than ZnO sample. Nevertheless, the intensity peaks for the ZnO/ 7 wt% Fe_3O_4 nanocomposite were the lowest as compared to other samples. ZnO/Fe_3O_4 nanocomposites have better separation of electron-hole pairs due to Fe^{3+} ions provided a photo-excited electron-trapping site and the photocatalysts lifetime were prolonged (Ambrus et al., 2008) (Ahmed, El-Katori and Gharni, 2013). Therefore, the heterojunction formation between ZnO and Fe_3O_4 semiconductors could improve the electron-hole separation efficiency. The results were also similar to other literatures (Shekofteh-Gohari and Habibi-Yangjeh, 2015) (Abazari, Mahjoub and Sanati, 2016) (Shekofteh-Gohari and Habibi-Yangjeh, 2017).

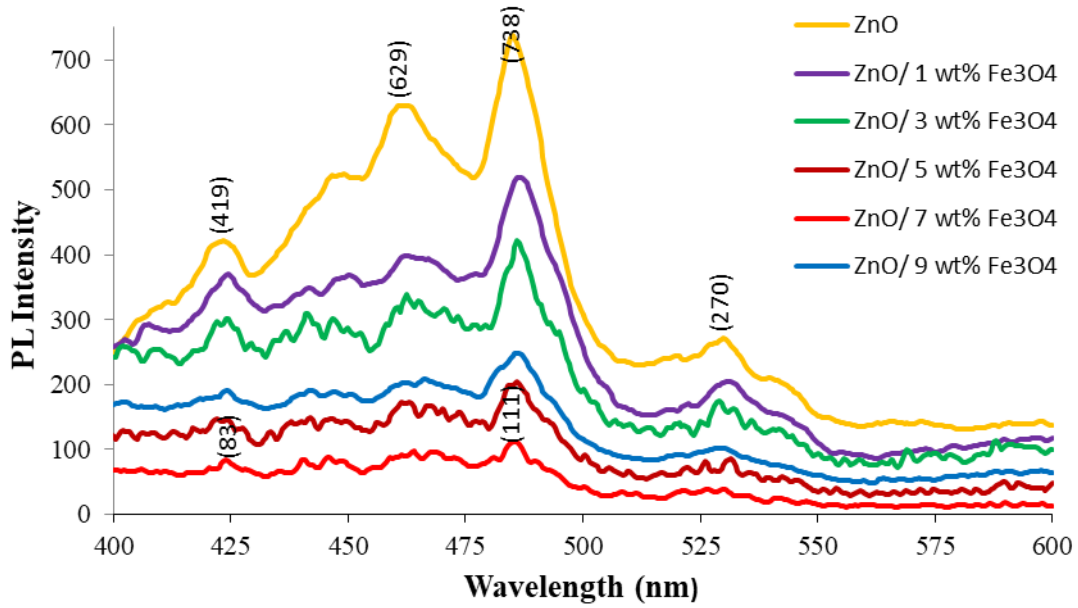

Figure 4.4: Photoluminescence spectra of ZnO, ZnO/ 1 wt% Fe_3O_4, ZnO/ 3 wt% Fe_3O_4, ZnO/ 5 wt% Fe_3O_4, ZnO/ 7 wt% Fe_3O_4, and ZnO/ 9 wt% Fe_3O_4

4.2 Control Experiment

The control experiments were demonstrated in order to evaluate the influence of the presence of catalyst and light towards photocatalysis, sonophotocatalysis and sonocatalysis reactions. As a result, the effect of catalysts and light irradiation on photocatalytic and sonophotocatalytic degradation of phenol was determined using 1.5 g/L ZnO/Fe_3O_4 catalyst loading and 20 ppm phenol concentration. While, for sonocatalytic degradation of phenol was determined using 1.0 g/L ZnO/Fe_3O_4 catalyst loading and 20 ppm phenol concentration of. The dark run without any light irradiation was demonstrated with catalyst to get the adsorption equilibrium. Besides, the photolysis was performed with light irradiation but absence of the catalyst. Photocatalysis, sonophotocatalysis and sonocatalysis were carried out with the use of catalyst. Figure 4.5 demonstrate the degradation efficiency of phenol under various conditions. Based on the results, the degradation efficiencies for both dark and photolysis run were very low as compared to photocatalysis, sonophotocatalysis and sonocatalysis reactions which were 1.5 % and 2.1 %.

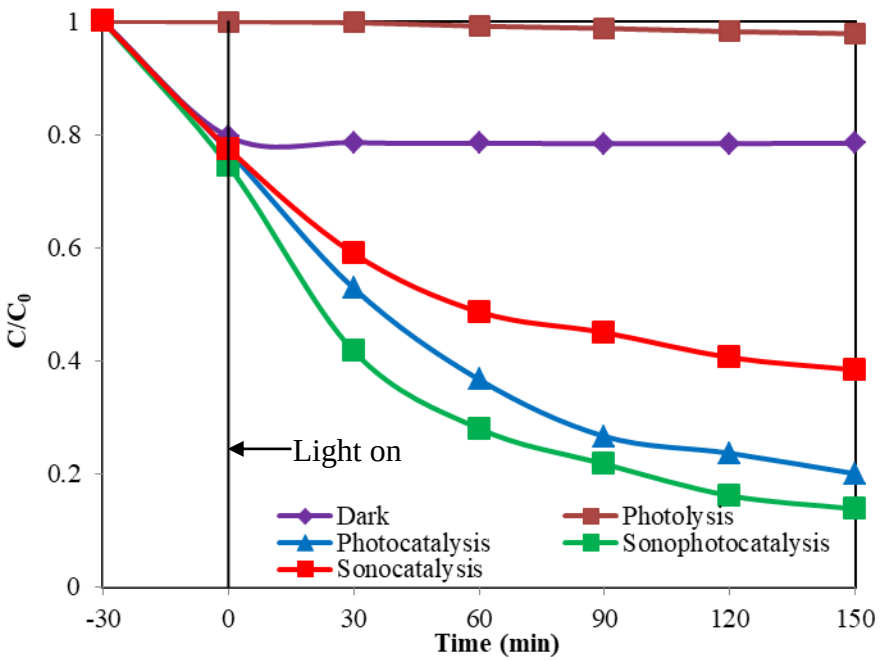

Figure 4.5: Removal of Phenol at Different Conditions. Conditions: Initial Phenol Concentrations = 20 ppm, Catalyst loading for Photocatalysis and Sonophotocatalysis = 1.5 g/L and Catalyst Loading for Sonocatalysis = 1.0 g/L.

The sonophotocatalysis has the highest degradation efficiency of 81.4 % as compared to photocatalysis and sonocatalysis which were 74.0 % and 50.4 % respectively. This proved that the combination of both ultrasonic and light irradiation have accelerated degradation efficiency as compared to photocatalysis and sonocatalysis due to the increase in the generation of •OH radicals. Hence, high degradation efficiency of phenol can be determined by the sonophotocatalysis reaction. Similar results also showed that the combination of both ultrasonic and light irradiation were required for the effective degradation efficiency (Ahmad et al., 2014; Bokhale et al., 2014).

4.3 Effect of Operating Parameters

4.3.1 Effect of Catalyst Loading

The optimum catalyst loading is an important factor to verify total photons absorption and avoid excess catalyst. Hence, the effect of catalyst loading was determined on photocatalysis, sonophotocatalysis and sonocatalysis of phenol over the ZnO/Fe_3O_4 catalyst. The catalyst loading experiment was carried out under the fluorescent lamp at constant initial phenol concentration of 20 ppm and solution pH of 5 by changing the amount of photocatalyst which were 0.5 g/L, 1.0 g/L, 1.5 g/L and 2.0 g/L. Figure 4.6 (a), (b) and (c) shows the phenol degradation efficiency with different catalyst loading for photocatalytic, sonophotocatalytic and sonocatalytic degradation.

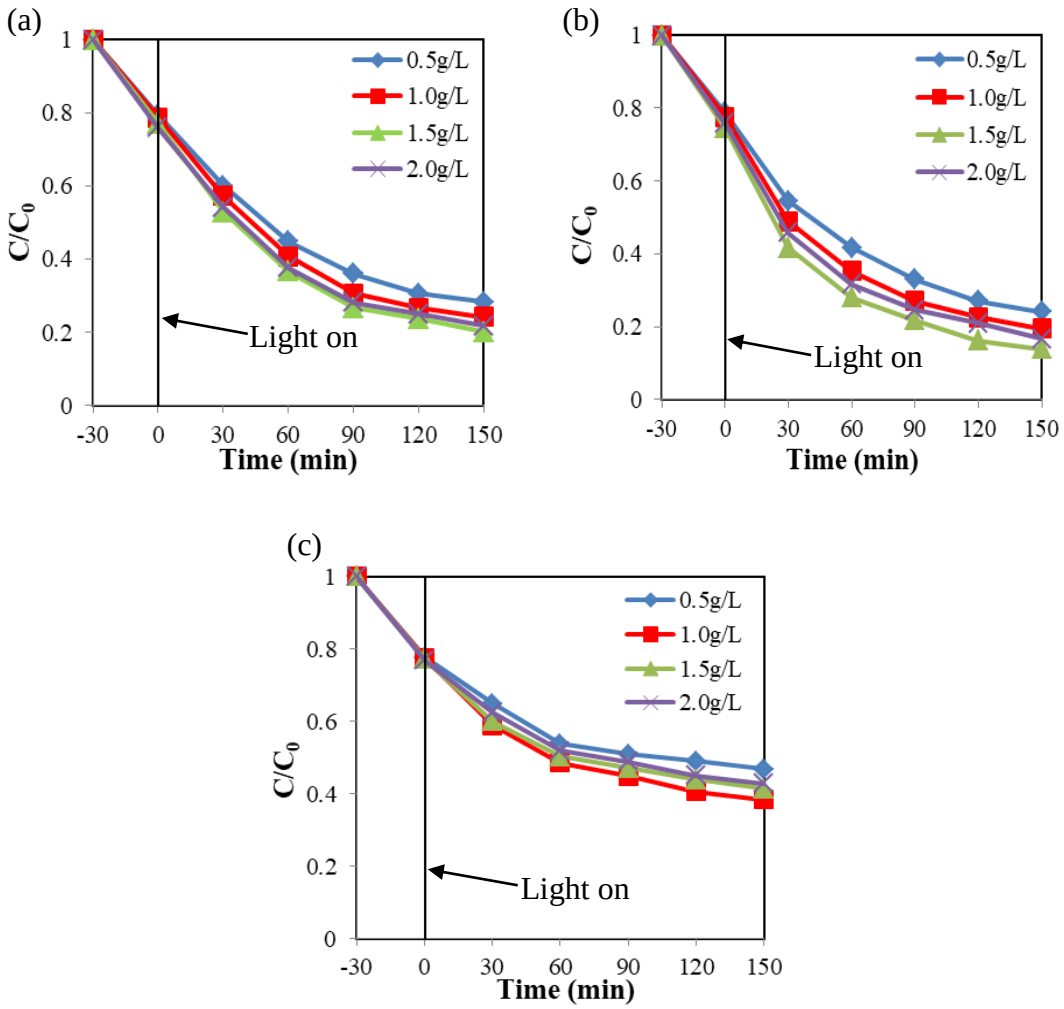

Figure 4.6: Effect of Catalyst Loading (a) Photocatalytic (b) Sonophotocatalytic and (c) Sonocatalytic. Conditions: Initial Phenol Concentration = 20 ppm, Solution pH = 5.

Based on the result, the photocatalytic degradation efficiency of phenol after 150 min of irradiation time had increased from 64.4 % to 73.9 % when catalyst loading increased from 0.5 g/L to 1.5 g/L. However, further increase the catalyst loading to 2.0 g/L, the degradation efficiency decreased to 71.4 %. Next, the sonophotocatalytic degradation efficiency of phenol after 150 min of irradiation time had increased from 69.5 % to 81.5 % when catalyst loading increased from 0.5 g/L to 1.5 g/L. Nevertheless, the phenol degradation efficiency decreased to 77.9 % when the catalyst loading reached 2.0 g/L. The sonocatalytic degradation efficiency of phenol increased from 39.7 % to 50.4 % when catalyst loading increased from 0.5 g/L to 1.0 g/L. However, further increase the ZnO/Fe_3O_4 loading to 1.5 g/L and 2.0 g/L, the degradation percentage decreased to 46.3 % and 44.3 % respectively. Thus,

the optimum ZnO/Fe_3O_4 loading for photocatalytic and sonophotocatalytic degradation was 1.5 g/L. The optimum ZnO/Fe_3O_4 loading for sonocatalytic degradation was 1.0 g/L.

In all three cases, the result of degradation efficiency increased can be explained with the increase of ZnO/Fe_eO_4 catalyst loading, amount of adsorption sites and active surface area. It will lead to generate more •OH radicals to degrade the phenol. Shah, Jan and Khitab (2018) found out that similar observation on the photocatalytic degradation of textile dyes over Cu impregnated ZnO catalyst in aqueous solution. They reported that high catalyst loading over the optimum condition can increase turbidity in the solution and reduced passage light to the molecule. Thereby, this will reduce adsorption of the substrate on the surface and caused a lower degradation rate. On the other hand, Tabasideh et al (2017) demonstrated the sonocatalytic degradation of diazinon in iron-doped TiO_2 nanoparticles aqueous solution. They found out that the •H radicals, •O radicals, and •OH radicals were generated in pyrolyzing water through ultrasonic irradiation. The produced radicals can react with diazinon in the bulk solution or interface between the bubbles and liquid phase. Radicals and hydrogen peroxide (H_2O_2) being produced thermolytic reactions of water and diazinon and nano-catalyst recombination. However, when the catalyst loading beyond this optimum range which was 0.4 g/L, the catalyst can agglomerate and reduced degradation efficiency of diazinon. Hence, overload of catalyst can decrease the catalytic degradation activity.

The degradation efficiency in sonophotocatalysis was higher than the photocatalysis for all catalyst loading. In sonophotocatalysis, the degradation efficiency decrease and catalyst loading increase over a maximum point was more significant as compared to photocatalysis. Ultrasonic promoted less •OH radicals generation and caused the degradation rate for sonophotocatalytic conditions at higher catalyst loadings decreased slightly (Anju, Yesodharan and Yesodharan, 2012). Moreover, Davydov et al (2001) also demonstrated for sonophotocatalysis, as the catalyst loading has reached the optimum conditions, higher ultrasonic power need to apply for the achievement and enhancement in reaction activity.

4.3.2 Effect of Initial Phenol Concentration

The effect of initial phenol concentration was analysed under the irradiation of fluorescent lamp for photocatalytic, sonophotocatalytic and sonocatalytic degradation over the synthesised ZnO/Fe_3O_4 catalysts. To study the effect of phenol concentration, a series of experiments were carried out at different phenol concentrations from 20 ppm to 60 ppm using constant 1.5 g/L catalyst loading and 5 pH solution for photocatalysis and sonophotocatalysis. While the catalyst loading and solution pH for sonocatalysis which were 1.0 g/L and solution pH of 5. Figure 4.7 (a), (b) and (c) shows the degradation efficiency of phenol with different initial phenol concentration for photocatalytic, sonophotocatalytic and sonocatalytic degradation. Based on the results, the optimum phenol concentrations achieved was 20 ppm (74.0 %) for photocatalysis while it was (81.4 %) for sonophotocatalysis and (50.4 %) for sonocatalysis. Besides, the tabulated results also found out that sonophotocatalysis have the highest degradation efficiency (81.4 %) as compared to photocatalysis and sonocatalysis at initial phenol concentration of 20 ppm.

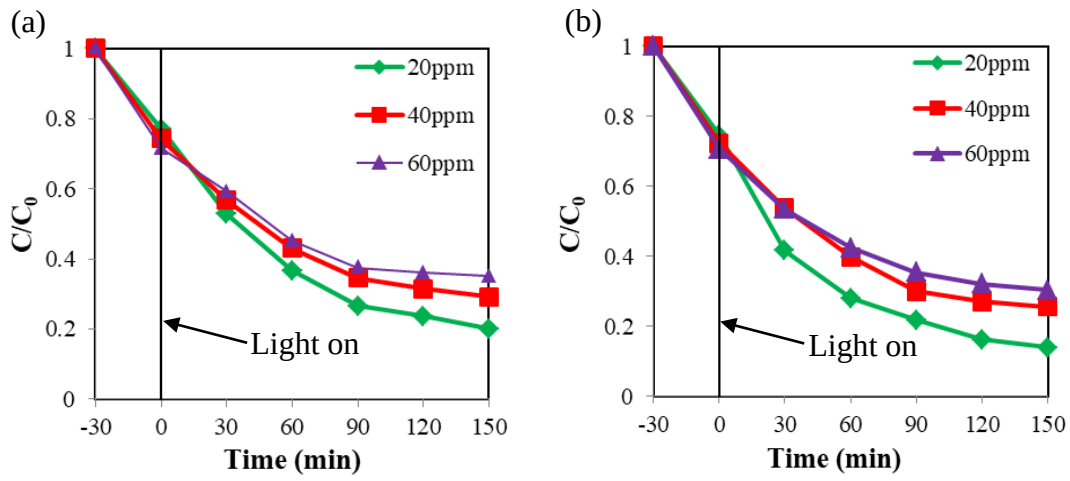

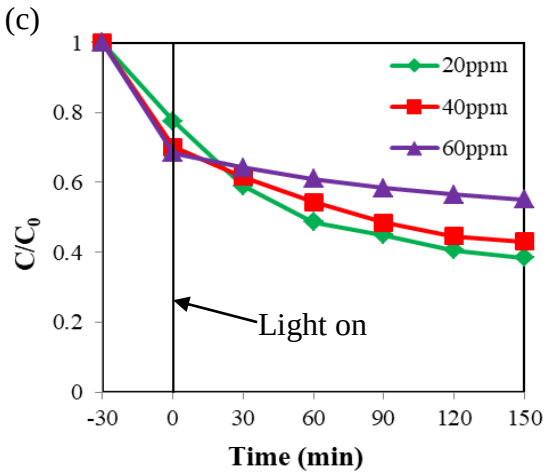

Figure 4.7: Effect of Initial Phenol Concentration (a) Photocatalytic, (b) Sonophotocatalytic and (c) Sonocatalytic. Conditions: Catalysts Loading = 1.5 g/L for (a) and (b), 1.0 g/L for (c), Solution pH = 5.

The results showed decreasing trend on the photocatalytic degradation efficiency when that is an increment of initial phenol concentration due to more reactant molecules concentration adsorbed on the surface of the catalyst. Hence, there is very low availability of the surface sites for the new generation of •OH radicals. The sonocatalytic degradation occurred in the large volume of the solution and it caused a low concentration of •OH radicals. Therefore, the catalyst saturation surface consumed longer time for the catalysts (Tabasideh et al., 2017). The decrease in degradation efficiency of phenol with the increasing the initial phenol concentration was due to the decrease in concentration of generated active radicals. With the high phenol concentration, more phenol molecules will be adsorbed to the active sites of the catalysts. Therefore, huge amount of phenol molecules were adsorbed on the catalyst surface and decreased the production rate of active radicals for phenol degradation (Daneshvar et al, 2007; Thennarasu and Sivasamy, 2016).

In photocatalytic degradation, increase in concentration will caused the adsorption of reactant molecules on catalyst site and interacted with •OH radicals. The adsorption carried out continuously until all the surface sites are occupied. Moreover, increase in concentration will not affect the result in increased of the surface occupation. However, sonocatalytic degradation has lower concentration of •OH radicals as it demonstrated in the bulk of the solution. Hence, limited •OH radicals leading to increase degradation efficiency when increase the phenol concentration. The sonocatalysis process will not be continued when the phenol

concentrations have reached optimum number of •OH radicals to interact (Anju, Yesodharan and Yesodharan, 2012).

4.3.3 Effect of Solution pH

The degradation efficiency for the photocatalysis of phenol after 150 min of light irradiation increased from 66.2 % to 74.0 % upon an increase in solution pH from 3 to 5. However, further increase in the solution pH to 7, 9 and 11 decreased the degradation efficiency to 69.0 %, 50.0 % and 36.0 %. The degradation efficiency for the sonophotocatalysis of phenol after 150 min of light irradiation increased from 73.4 % to 81.5 % upon an increase in solution pH from 3 to 5. However, the solution pH further increased to 7, 9 and 11, caused a reduction of degradation efficiency to 75.8 %, 59.5 % and 40.6 %. Next, the degradation efficiency for the sonocatalysis of phenol after 150 min of light irradiation increased from 41.68% to 50.43% upon an increase in solution pH from 3 to 5. However, the solution pH further increased to 7, 9 and 11, caused a reduction of degradation efficiency 46.32%, 30.67% and 20.75%. Figure 4.8 (a), (b) and (c) shows the effect of solution pH on the photocatalysis, sonophotocatalysis and sonocatalysis over ZnO/Fe_3O_4 photocatalysts.

(a)

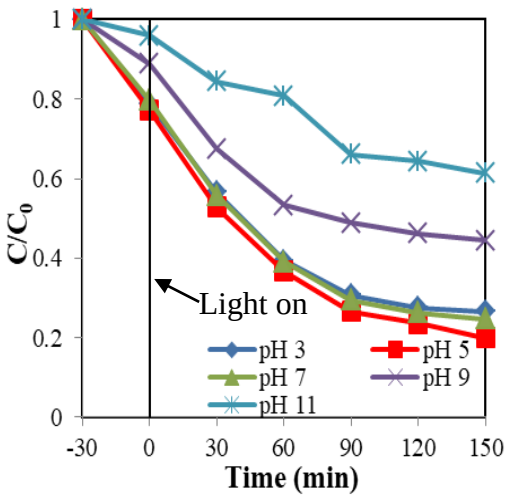

(b)

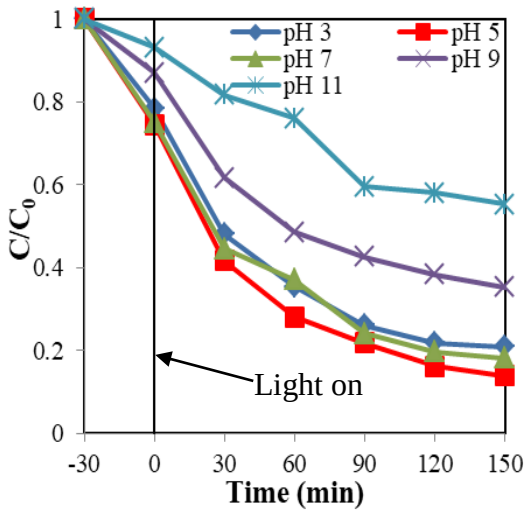

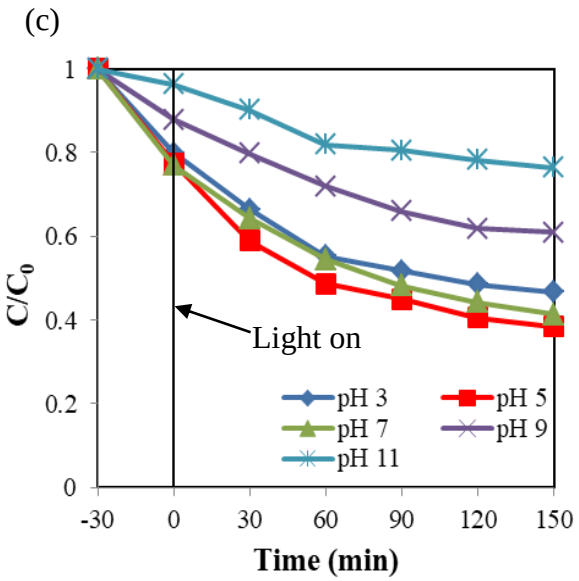

Figure 4.8: Effect of Solution pH (a) Photocatalytic, (b) Sonophotocatalytic and (c) Sonocatalytic. Conditions: Initial Phenol Concentration = 20 ppm, Catalysts Loading = 1.5 g/L for (a) and (b), 1.0 g/L for (c).

The ultrasonic and ultraviolet degradation of organic were affected on the pH value of the solution. Anju, Yesodharan and Yesodharan (2012) found out that the degradation was more efficient in acidic phase as compared to alkaline phase. They reported that the acidic pH range from 4 to 5.5 for sonophotocatalysis have a conversion of 85% while it is around 60% in alkaline conditions. The effect of solution pH can be determined according to amphoteric behaviour and surface charge of ZnO. The Point of Zero Charge (PZC) of ZnO was approximately 9 ± 0.3. Hence, this shows that the surface of ZnO is negatively charged when the pH value is higher than PZC value and positively charged when the pH value is lower (Bechambi, Sayadi and Najjar, 2015; Shah, Jan and Khitab, 2018). Next, Wu et al (2001) also reported that sonophotocatalytic degradation of phenol in presence of TiO_2 with the conversion of 98% in acidic range. However, it was only 60% in alkaline range. ZnO having a lower degradation rate below pH 4 due to more corrosion in acidic conditions resulting reduced catalytic activity and decreased concentration.

In the alkaline pH conditions, the adsorption of ZnO reduced due to phenol was in ionised form and it reduced the surface mediated degradation. Nevertheless, in acidic pH range, phenol remained in neutral form which will increase the ZnO

adsorption through active surface species and •OH radicals that produced in the aqueous solution (Saien and Soleymani, 2007). Furthermore, the presence of protons can initiate the formation of reactive •OH radicals from the available OH ions. Sonophotocatalysis can also be assigned to reduce the distance of the substrate molecule and catalyst particles surface to the effect of ultrasonic for a significant enhancement in the degradation (Saien, Delavari and Solymani, 2010). Substrated adsorption on the catalyst surface and the •OH radical formation was the important factors for the degradation efficiency (Anju, Yesodharan and Yesodharan, 2012). In conclusion, the highest photocatalytic, sonophotocatalytic and sonocatalytic degradation efficiency of phenol over synthesised ZnO/Fe_3O_4 catalyst was achieved at the solution pH of 5 after 150 min light irradiation.

CHAPTER 5

CONCLUSION AND RECOMMENDATIONS

5.1 Conclusion

In this study, we evaluated sonocatalytic, photocatalytic, and sonophotocatalytic degradation of phenol using synthesised magnetic separable ZnO/Fe_3O_4 photocatalysts via chemical precipitation deposition method and characterised using different techniques. The X-Ray diffraction (XRD) of synthesised ZnO/Fe_3O_4 catalysts showed its well-crystalline and hexagonal wurtzite structure. The fourier transform infrared (FTIR) spectrum showed the successfully coupling of ZnO/Fe_3O_4 catalysts with the functional groups of Zn-O and Fe-O. In addition, the scanning electron microscopy (SEM) images revealed the surface morphology of the ZnO/Fe_3O_4 composites had hierarchical structures. The energy dispersive X-ray (EDX) spectroscopy images showed the distribution of Fe_3O_4 on the surface of ZnO surface. The photoluminescence (PL) spectroscopy showed the electronic properties of the ZnO/Fe_3O_4 catalysts.

The control experiment of sonocatalytic, photocatalytic, and sonophotocatalytic degradation of phenol showed that high degradation efficiency by ZnO/Fe_3O_4 catalysts as compared to dark adsorption and photolysis. Moreover, this study showed that the reactions that carried out in this experiment were sonocatalysis, photocatalysis and sonophotocatalysis. The optimum degradation of phenol was investigated in terms of initial phenol concentration, catalyst loading and solution pH. From the results, sonophotocatalytic degradation exhibited better degradation performance under visible light in the presence of ultrasound as compared to

photocatalytic and sonocatalytic degradation. The cavitation energy of ultrasounds increased the concentration of oxidizing agents which have improved the sonophotocatalytic degradation process. The 1.5 g/L was the optimum catalyst loading to require a high degradation efficiency of phenol. Besides, the optimum initial phenol concentration of 20 ppm was needed to acquire highest degradation efficiency for sonophotocatalysis. Non-adjustment for solution pH of phenol was added has achieved the highest sonophotocatalytic degradation efficiency and optimum pH was found to be 5.

5.2 Recommendations

There are several recommendations were suggested for future studies:

1. Studies on more operating parameters such as presence of surfactants in solution, inorganic anion and cation which can investigate optimum condition for ZnO/Fe_3O_4 composites to carry out sonophotocatalytic degradation
2. In this study, sonophotocatalytic degradation using fluorescent lamp consist an effective method to degrade phenol. For future research should be carried out by sunlight to study the sonophotocatalytic degradation efficiency.

REFERENCES

Abazari, R., Mahjoub, A. and Sanati, S. (2016). Magnetically recoverable Fe 3 O 4 - ZnO/AOT nanocomposites: Synthesis of a core–shell structure via a novel and mild route for photocatalytic degradation of toxic dyes. *Journal of Molecular Liquids*, 223, pp.1133-1142.

Afroz, R., Hassan, M. and Ibrahim, N. (2003). Review of air pollution and health impacts in Malaysia. *Environmental Research*, 92(2), pp.71-77.

Agustina, T., Ang, H. and Vareek, V. (2005). A review of synergistic effect of photocatalysis and ozonation on wastewater treatment. *Journal of Photochemistry and Photobiology C: Photochemistry Reviews*, 6(4), pp.264-273.

Ahmad, M., Ahmed, E., Hong, Z., Ahmed, W., Elhissi, A. and Khalid, N. (2014). Photocatalytic, sonocatalytic and sonophotocatalytic degradation of Rhodamine B using ZnO/CNTs composites photocatalysts. *Ultrasonics Sonochemistry*, 21(2), pp.761-773.

Ahmed, M., El-Katori, E. and Gharni, Z. (2013). Photocatalytic degradation of methylene blue dye using Fe2O3/TiO2 nanoparticles prepared by sol–gel method. *Journal of Alloys and Compounds*, 553, pp.19-29.

Ahmed, S., Rasul, M., Brown, R. and Hashib, M. (2011). Influence of parameters on the heterogeneous photocatalytic degradation of pesticides and phenolic contaminants in wastewater: A short review. *Journal of Environmental Management*, 92(3), pp.311-330.

Ahmed, S., Rasul, M., Martens, W., Brown, R. and Hashib, M. (2010). Advances in Heterogeneous Photocatalytic Degradation of Phenols and Dyes in Wastewater: A Review. *Water, Air, & Soil Pollution*, 215(1-4), pp.3-29.

Ambrus, Z., Balázs, N., Alapi, T., Wittmann, G., Sipos, P., Dombi, A. and Mogyorósi, K. (2008). Synthesis, structure and photocatalytic properties of Fe(III)-doped TiO2 prepared from TiCl3. *Applied Catalysis B: Environmental*, 81(1-2), pp.27-37.

Andreozzi, R. (1999). Advanced oxidation processes (AOP) for water purification and recovery. *Catalysis Today*, 53(1), pp.51-59.

Anju, S., Yesodharan, S. and Yesodharan, E. (2012). Zinc oxide mediated sonophotocatalytic degradation of phenol in water. *Chemical Engineering Journal*, 189-190, pp.84-93.

Anjum, M., Oves, M., Kumar, R. and Barakat, M. (2017). Fabrication of ZnO-ZnS@polyaniline nanohybrid for enhanced photocatalytic degradation of 2-chlorophenol and microbial contaminants in wastewater. *International Biodeterioration & Biodegradation*, 119, pp.66-77.

Ariffin, M. and Sulaiman, S. (2015). Regulating Sewage Pollution of Malaysian Rivers and its Challenges. *Procedia Environmental Sciences*, 30, pp.168-173.

Asgari, S., Fakhari, Z. and Berijani, S., 2014. Synthesis and Characterization of Fe3O4 Magnetic Nanoparticles Coated with Carboxymethyl Chitosan Grafted Sodium Methacrylate. *Journal of Nanostructures*, *4*(1), pp.55-63.

Asghar, A., Abdul Raman, A. and Wan Daud, W. (2015). Advanced oxidation processes for in-situ production of hydrogen peroxide/hydroxyl radical for textile wastewater treatment: a review. *Journal of Cleaner Production*, 87, pp.826-838.

Ashar, A., Iqbal, M., Bhatti, I., Ahmad, M., Qureshi, K., Nisar, J. and Bukhari, I. (2016). Synthesis, characterization and photocatalytic activity of ZnO flower and pseudo-sphere: Nonylphenol ethoxylate degradation under UV and solar irradiation. *Journal of Alloys and Compounds*, 678, pp.126-136.

Augugliaro, V., Palmisano, L., Sclafani, A., Minero, C. and Pelizzetti, E. (1988). Photocatalytic degradation of phenol in aqueous titanium dioxide dispersions. *Toxicological & Environmental Chemistry*, 16(2), pp.89-109.

Bechambi, O., Najjar, W. and Sayadi, S. (2016). The nonylphenol degradation under UV irradiation in the presence of Ag–ZnO nanorods: Effect of parameters and degradation pathway. *Journal of the Taiwan Institute of Chemical Engineers*, 60, pp.496-501.

Bechambi, O., Sayadi, S. and Najjar, W. (2015). Photocatalytic degradation of bisphenol A in the presence of C-doped ZnO: Effect of operational parameters and photodegradation mechanism. *Journal of Industrial and Engineering Chemistry*, 32, pp.201-210.

Bokhale, N., Bomble, S., Dalbhanjan, R., Mahale, D., Hinge, S., Banerjee, B., Mohod, A. and Gogate, P. (2014). Sonocatalytic and sonophotocatalytic degradation of rhodamine 6G containing wastewaters. *Ultrasonics Sonochemistry*, 21(5), pp.1797-1804.

Busca, G., Berardinelli, S., Resini, C. and Arrighi, L. (2008). Technologies for the removal of phenol from fluid streams: A short review of recent developments. *Journal of Hazardous Materials*, 160(2-3), pp.265-288.

Bustos-Torres, K., Vazquez-Rodriguez, S., la Cruz, A., Sepulveda-Guzman, S., Benavides, R., Lopez-Gonzalez, R. and Torres-Martínez, L. (2017). Influence of the morphology of ZnO nanomaterials on photooxidation of polypropylene/ZnO composites. *Materials Science in Semiconductor Processing*, 68, pp.217-225.

Casillas, J., Tzompantzi, F., Castellanos, S., Mendoza-Damián, G., Pérez-Hernández, R., López-Gaona, A. and Barrera, A. (2017). Promotion effect of ZnO on the photocatalytic activity of coupled Al 2 O 3 -Nd 2 O 3 -ZnO composites prepared by the sol − gel method in the degradation of phenol. *Applied Catalysis B: Environmental*, 208, pp.161-170.

Chalasani, R. and Vasudevan, S. (2013). Cyclodextrin-Functionalized Fe3O4@TiO2: Reusable, Magnetic Nanoparticles for Photocatalytic Degradation of Endocrine-Disrupting Chemicals in Water Supplies. *ACS Nano*, 7(5), pp.4093-4104.

Daneshvar, N., Rasoulifard, M., Khataee, A. and Hosseinzadeh, F. (2007). Removal of C.I. Acid Orange 7 from aqueous solution by UV irradiation in the presence of ZnO nanopowder. *Journal of Hazardous Materials*, 143(1-2), pp.95-101.

Daneshvar, N., Salari, D. and Khataee, A. (2004). Photocatalytic degradation of azo dye acid red 14 in water on ZnO as an alternative catalyst to TiO2. *Journal of Photochemistry and Photobiology A: Chemistry*, 162(2-3), pp.317-322.

Darvishi Cheshmeh Soltani, R., Jorfi, S., Ramezani, H. and Purfadakari, S. (2016). Ultrasonically induced ZnO–biosilica nanocomposite for degradation of a textile dye in aqueous phase. *Ultrasonics Sonochemistry*, 28, pp.69-78.

Darvishi Cheshmeh Soltani, R., Jorfi, S., Safari, M. and Rajaei, M. (2016). Enhanced sonocatalysis of textile wastewater using bentonite-supported ZnO nanoparticles: Response surface methodological approach. *Journal of Environmental Management*, 179, pp.47-57.

Davydov, L., Reddy, E., France, P. and Smirniotis, P. (2001). Sonophotocatalytic destruction of organic contaminants in aqueous systems on TiO2 powders. *Applied Catalysis B: Environmental*, 32(1-2), pp.95-105.

Dewidar, H., Nosier, S. and El-Shazly, A. (2018). Photocatalytic degradation of phenol solution using Zinc Oxide/UV. *Journal of Chemical Health and Safety*, 25(1), pp.2-11.

Dong, S., Xu, K., Wei, C. and Liu, J. (2011). Effect of 3D ZnO:Fe morphology on the photocatalytic activity under solar irradiation. *Research on Chemical Intermediates*, 38(3-5), pp.1055-1062.

ElShafei, G., Al-Sabagh, A., Yehia, F., Philip, C., Moussa, N., Eshaq, G. and ElMetwally, A. (2018). Metal oxychlorides as robust heterogeneous Fenton catalysts for the sonophotocatalytic degradation of 2-nitrophenol. *Applied Catalysis B: Environmental*, 224, pp.681-691.

Farrokhi, M., Hosseini, S., Yang, J. and Shirzad-Siboni, M. (2014). Application of ZnO–Fe3O4 Nanocomposite on the Removal of Azo Dye from Aqueous Solutions: Kinetics and Equilibrium Studies. *Water, Air, & Soil Pollution*, 225(9).

Fatimah, I. and Novitasari (2016). Preparation of TiO2-ZnO and its activity test in sonophotocatalytic degradation of phenol. *IOP Conference Series: Materials Science and Engineering*, 107, p.012003.

Fatimah, Is & Yulia Pradita, Rizqi & Nurfalinda, Annisa. (2017). Study on ZnO Catalytic Activity in Salycilic Acid Degradation by Sonophotocatalysis. Chemical Engineering Transactions.

Feng, X., Guo, H., Patel, K., Zhou, H. and Lou, X. (2014). High performance, recoverable Fe3O4ZnO nanoparticles for enhanced photocatalytic degradation of phenol. *Chemical Engineering Journal*, 244, pp.327-334.

Gaya, U., Abdullah, A., Zainal, Z. and Hussein, M. (2009). Photocatalytic treatment of 4-chlorophenol in aqueous ZnO suspensions: Intermediates, influence of dosage and inorganic anions. *Journal of Hazardous Materials*, 168(1), pp.57-63.

Gharagozlou, M. and Naghibi, S. (2018). Sensitization of ZnO nanoparticles by metal–free phthalocyanine. *Journal of Luminescence*, 196, pp.64-68.

Guo, J., Ma, B., Yin, A., Fan, K. and Dai, W. (2011). Photodegradation of rhodamine B and 4-chlorophenol using plasmonic photocatalyst of Ag–AgI/Fe3O4@SiO2 magnetic nanoparticle under visible light irradiation. *Applied Catalysis B: Environmental*, 101(3-4), pp.580-586.

Guo, M., Ng, A., Liu, F., Djurišić, A., Chan, W., Su, H. and Wong, K. (2011). Effect of Native Defects on Photocatalytic Properties of ZnO. *The Journal of Physical Chemistry C*, 115(22), pp.11095-11101.

Habibi-Yangjeh, A. and Shekofteh-Gohari, M. (2016). Fe 3 O 4 /ZnO/Ag 3 VO 4 /AgI nanocomposites: Quaternary magnetic photocatalysts with excellent activity in degradation of water pollutants under visible light. *Separation and Purification Technology*, 166, pp.63-72.

Han, J., Liu, Y., Singhal, N., Wang, L. and Gao, W. (2012). Comparative photocatalytic degradation of estrone in water by ZnO and TiO2 under artificial UVA and solar irradiation. *Chemical Engineering Journal*, 213, pp.150-162.

Hao, J., Ji, L., Wu, K. and Yang, N. (2018). Electrochemistry of ZnO@reduced graphene oxides. *Carbon*, 130, pp.480-486.

Haque, M., Muneer, M. and Bahnemann, D. (2006). Semiconductor-Mediated Photocatalyzed Degradation of a Herbicide Derivative, Chlorotoluron, in Aqueous Suspensions. *Environmental Science & Technology*, 40(15), pp.4765-4770.

Hassan, F. (2011). Photochemical Treatments of Textile Industries Wastewater. *Advances in Treating Textile Effluent*.

Hitkari, G., Singh, S. and Pandey, G. (2017). Structural, optical and photocatalytic study of ZnO and ZnO–ZnS synthesized by chemical method. *Nano-Structures & Nano-Objects*, 12, pp.1-9.

Hong, R., Zhang, S., Di, G., Li, H., Zheng, Y., Ding, J. and Wei, D. (2008). Preparation, characterization and application of Fe3O4/ZnO core/shell magnetic nanoparticles. *Materials Research Bulletin*, 43(8-9), pp.2457-2468.

Hu, B., Wu, C., Zhang, Z. and Wang, L. (2014). Sonophotocatalytic degradation of trichloroacetic acid in aqueous solution. *Ceramics International*, 40(5), pp.7015-7021.

Huang, C., Dong, C. and Tang, Z. (1993). Advanced chemical oxidation: Its present role and potential future in hazardous waste treatment. *Waste Management*, 13(5-7), pp.361-377.

Jiang, J., Zhao, P., Shi, L., Yue, X., Qiu, Q., Xie, T., Wang, D., Lin, Y. and Mu, Z. (2018). Insights into the interface effect in Pt@BiOI/ZnO ternary hybrid composite for efficient photodegradation of phenol and photogenerated charge transfer properties. *Journal of Colloid and Interface Science*, 518, pp.102-110.

Jyothi, K., Yesodharan, S. and Yesodharan, E. (2014). Ultrasound (US), Ultraviolet light (UV) and combination (US+UV) assisted semiconductor catalysed degradation of organic pollutants in water: Oscillation in the concentration of hydrogen peroxide formed in situ. *Ultrasonics Sonochemistry*, 21(5), pp.1787-1796.

Kahouli, M., Barhoumi, A., Bouzid, A., Al-Hajry, A. and Guermazi, S. (2015). Structural and optical properties of ZnO nanoparticles prepared by direct precipitation method. *Superlattices and Microstructures*, 85, pp.7-23.

Kansal, S., Singh, M. and Sud, D. (2008). Studies on TiO2/ZnO photocatalysed degradation of lignin. *Journal of Hazardous Materials*, 153(1-2), pp.412-417.

Kaur, J., Bansal, S. and Singhal, S. (2013). Photocatalytic degradation of methyl orange using ZnO nanopowders synthesized via thermal decomposition of oxalate precursor method. *Physica B: Condensed Matter*, 416, pp.33-38.

Khataee, A., Arefi-Oskoui, S. and Samaei, L. (2018). ZnFe-Cl nanolayered double hydroxide as a novel catalyst for sonocatalytic degradation of an organic dye. *Ultrasonics Sonochemistry*, 40, pp.703-713.

Khataee, A., Hassandoost, R. and Rahim Pouran, S. (2018). Cerium-substituted magnetite: Fabrication, characterization and sonocatalytic activity assessment. *Ultrasonics Sonochemistry*, 41, pp.626-640.

Khataee, A., Kayan, B., Gholami, P., Kalderis, D. and Akay, S. (2017). Sonocatalytic degradation of an anthraquinone dye using TiO 2 -biochar nanocomposite. *Ultrasonics Sonochemistry*, 39, pp.120-128.

Khataee, A., Mohamadi, F., Rad, T. and Vahid, B. (2018). Heterogeneous sonocatalytic degradation of anazolene sodium by synthesized dysprosium doped CdSe nanostructures. *Ultrasonics Sonochemistry*, 40, pp.361-372.

Khodja, A., Sehili, T., Pilichowski, J. and Boule, P. (2001). Photocatalytic degradation of 2-phenylphenol on TiO2 and ZnO in aqueous suspensions. *Journal of Photochemistry and Photobiology A: Chemistry*, 141(2-3), pp.231-239.

Kumar, P., Som, S., Pandey, M., Das, S., Chanda, A. and Singh, J. (2018). Investigations on optical properties of ZnO decorated graphene oxide (ZnO@GO) and reduced graphene oxide (ZnO@r-GO). *Journal of Alloys and Compounds*, 744, pp.64-74.

Kwon, C. (2004). Degradation of methylene blue via photocatalysis of titanium dioxide. *Materials Chemistry and Physics*, 86(1), pp.78-82.

Lam, S., Sin, J., Abdullah, A. and Mohamed, A. (2012). Degradation of wastewaters containing organic dyes photocatalysed by zinc oxide: a review. *Desalination and Water Treatment*, 41(1-3), pp.131-169.

Lathasree, S., Rao, A., SivaSankar, B., Sadasivam, V. and Rengaraj, K. (2004). Heterogeneous photocatalytic mineralisation of phenols in aqueous solutions. *Journal of Molecular Catalysis A: Chemical*, 223(1-2), pp.101-105.

Lavand, A. and Malghe, Y. (2015). Visible light photocatalytic degradation of 4-chlorophenol using C/ZnO/CdS nanocomposite. *Journal of Saudi Chemical Society*, 19(5), pp.471-478.

Lee, K., Abd Hamid, S. and Lai, C. (2015). Mechanism and Kinetics Study for Photocatalytic Oxidation Degradation: A Case Study for Phenoxyacetic Acid Organic Pollutant. *Journal of Nanomaterials*, 2015, pp.1-10.

Lee, K., Lai, C., Ngai, K. and Juan, J. (2016). Recent developments of zinc oxide based photocatalyst in water treatment technology: A review. *Water Research*, 88, pp.428-448.

Lei, A., Qu, B., Zhou, W., Wang, Y., Zhang, Q. and Zou, B. (2012). Facile synthesis and enhanced photocatalytic activity of hierarchical porous ZnO microspheres. *Materials Letters*, 66(1), pp.72-75.

Li, D. and Haneda, H. (2003). Morphologies of zinc oxide particles and their effects on photocatalysis. *Chemosphere*, 51(2), pp.129-137.

Li, S., Wang, G., Qiao, J., Zhou, Y., Ma, X., Zhang, H., Li, G., Wang, J. and Song, Y. (2018). Sonocatalytic degradation of norfloxacin in aqueous solution caused by a novel Z-scheme sonocatalyst, mMBIP-MWCNT-In 2 O 3 composite. *Journal of Molecular Liquids*.

Linsebigler, A., Lu, G. and Yates, J. (1995). Photocatalysis on TiO2 Surfaces: Principles, Mechanisms, and Selected Results. *Chemical Reviews*, 95(3), pp.735-758.

Lu, H., Wang, S., Zhao, L., Li, J., Dong, B. and Xu, Z. (2011). Hierarchical ZnO microarchitectures assembled by ultrathin nanosheets: hydrothermal synthesis and enhanced photocatalytic activity. *Journal of Materials Chemistry*, 21(12), p.4228.

Ma, D., Zou, D., Zhou, D., Li, T., Dong, S., Xu, Z. and Dong, S. (2015). Phenol removal and biofilm response in coupling of visible-light-driven photocatalysis and biodegradation: Effect of hydrothermal treatment temperature. *International Biodeterioration & Biodegradation*, 104, pp.178-185.

Mahmoud, S. and Fouad, O. (2015). Synthesis and application of zinc/tin oxide nanostructures in photocatalysis and dye sensitized solar cells. *Solar Energy Materials and Solar Cells*, 136, pp.38-43.

May-Lozano, M., Mendoza-Escamilla, V., Rojas-García, E., López-Medina, R., Rivadeneyra-Romero, G. and Martinez-Delgadillo, S. (2017). Sonophotocatalytic degradation of Orange II dye using low cost photocatalyst. *Journal of Cleaner Production*, 148, pp.836-844.

Modirshahla, N., Hassani, A., Behnajady, M. and Rahbarfam, R. (2011). Effect of operational parameters on decolorization of Acid Yellow 23 from wastewater by UV irradiation using ZnO and ZnO/SnO2 photocatalysts. *Desalination*, 271(1-3), pp.187-192.

Mohajerani, M., Lak, A. and Simchi, A. (2009). Effect of morphology on the solar photocatalytic behavior of ZnO nanostructures. *Journal of Alloys and Compounds*, 485(1-2), pp.616-620.

Mohler, E. and Jacob, L. (1957). Determination of Phenolic-Type Compounds in Water and Industrial Waste Waters Comparison of Analytical Methods. *Analytical Chemistry*, 29(9), pp.1369-1374.

Mu, R., Xu, Z., Li, L., Shao, Y., Wan, H. and Zheng, S. (2010). On the photocatalytic properties of elongated TiO2 nanoparticles for phenol degradation and Cr(VI) reduction. *Journal of Hazardous Materials*, 176(1-3), pp.495-502.

Mukhopadhyay, S., Das, P., Maity, S., Ghosh, P. and Devi, P. (2015). Solution grown ZnO rods: Synthesis, characterization and defect mediated photocatalytic activity. *Applied Catalysis B: Environmental*, 165, pp.128-138.

Munter, R. (2001). Advanced Oxidation Processes: Current Status and Prospects. *ChemInform*, 32(41), pp.59-80.

Munter, R. (2010). ChemInform Abstract: Advanced Oxidation Processes: Current Status and Prospects. *ChemInform*, 32(41), pp.59-80.

Muyibi, S., Ambali, A. and Eissa, G. (2007). The Impact of Economic Development on Water Pollution: Trends and Policy Actions in Malaysia. *Water Resources Management*, 22(4), pp.485-508.

Nezamzadeh-Ejhieh, A. and Khorsandi, S. (2014). Photocatalytic degradation of 4-nitrophenol with ZnO supported nano-clinoptilolite zeolite. *Journal of Industrial and Engineering Chemistry*, 20(3), pp.937-946.

Özgür, Ü., Alivov, Y., Liu, C., Teke, A., Reshchikov, M., Doğan, S., Avrutin, V., Cho, S. and Morkoç, H. (2005). A comprehensive review of ZnO materials and devices. *Journal of Applied Physics*, 98(4), p.041301.

Pandiyarajan, T., Baesso, M. and Karthikeyan, B. (2014). Enhanced ultraviolet-blue emission and Raman modes in ZnO:Cr2O3 composite nanoparticles. *The European Physical Journal D*, 68(2).

Pardeshi, S. and Patil, A. (2008). A simple route for photocatalytic degradation of phenol in aqueous zinc oxide suspension using solar energy. *Solar Energy*, 82(8), pp.700-705.

Parida, K. and Parija, S. (2006). Photocatalytic degradation of phenol under solar radiation using microwave irradiated zinc oxide. *Solar Energy*, 80(8), pp.1048-1054.

Qin, Y., Zhang, H., Tong, Z., Song, Z. and Chen, N. (2017). A facile synthesis of Fe 3 O 4 @SiO 2 @ZnO with superior photocatalytic performance of 4-nitrophenol. *Journal of Environmental Chemical Engineering*, 5(3), pp.2207-2213.

Raj, K. and Sadayandi, K. (2016). Effect of temperature on structural, optical and photoluminescence studies on ZnO nanoparticles synthesized by the standard co-precipitation method. *Physica B: Condensed Matter*, 487, pp.1-7.

Ribeiro, A., Nunes, O., Pereira, M. and Silva, A. (2015). An overview on the advanced oxidation processes applied for the treatment of water pollutants defined in the recently launched Directive 2013/39/EU. *Environment International*, 75, pp.33-51.

Saffari, J., Mir, N., Ghanbari, D., Khandan-Barani, K., Hassanabadi, A. and Hosseini-Tabatabaei, M. (2015). Sonochemical synthesis of Fe3O4/ZnO magnetic nanocomposites and their application in photo-catalytic degradation of various organic dyes. *Journal of Materials Science: Materials in Electronics*, 26(12), pp.9591-9599.

Saien, J. and Soleymani, A. (2007). Degradation and mineralization of Direct Blue 71 in a circulating upflow reactor by UV/TiO2 process and employing a new method in kinetic study. *Journal of Hazardous Materials*, 144(1-2), pp.506-512.

Saien, J., Delavari, H. and Solymani, A. (2010). Sono-assisted photocatalytic degradation of styrene-acrylic acid copolymer in aqueous media with nano titania particles and kinetic studies. *Journal of Hazardous Materials*, 177(1-3), pp.1031-1038.

Sajjadi, S., Khataee, A. and Kamali, M. (2017). Sonocatalytic degradation of methylene blue by a novel graphene quantum dots anchored CdSe nanocatalyst. *Ultrasonics Sonochemistry*, 39, pp.676-685.

Salavati, H., Tavakkoli, N. and Hosseinpoor, M. (2012). Preparation and characterization of polyphosphotungstate/ZrO2 nanocomposite and their sonocatalytic and photocatalytic activity under UV light illumination. *Ultrasonics Sonochemistry*, 19(3), pp.546-553.

Salim, N., Jaafar, J., Ismail, A., Othman, M., Rahman, M., Yusof, N., Qtaishat, M., Matsuura, T., Aziz, F. and Salleh, W. (2018). Preparation and characterization of hydrophilic surface modifier macromolecule modified poly (ether sulfone) photocatalytic membrane for phenol removal. *Chemical Engineering Journal*, 335, pp.236-247.

Schiavello, M. (1993). Some working principles of heterogeneous photocatalysis by semiconductors. *Electrochimica Acta*, 38(1), pp.11-14.

Selvam, N., Narayanan, S., Kennedy, L. and Vijaya, J. (2013). Pure and Mg-doped self-assembled ZnO nano-particles for the enhanced photocatalytic degradation of 4-chlorophenol. *Journal of Environmental Sciences*, 25(10), pp.2157-2167.

Shah, J., Jan, M. and Khitab, F. (2018). Sonophotocatalytic degradation of textile dyes over Cu impregnated ZnO catalyst in aqueous solution. *Process Safety and Environmental Protection*, 116, pp.149-158.

Shekofteh-Gohari, M. and Habibi-Yangjeh, A. (2015). Ternary ZnO/Ag3VO4/Fe3O4 nanocomposites: Novel magnetically separable photocatalyst for efficiently degradation of dye pollutants under visible-light irradiation. *Solid State Sciences,* 48, pp.177-185.

Shekofteh-Gohari, M. and Habibi-Yangjeh, A. (2016). Fabrication of novel magnetically separable visible-light-driven photocatalysts through photosensitization of Fe 3 O 4 /ZnO with CuWO 4. *Journal of Industrial and Engineering Chemistry*, 44, pp.174-184.

Shekofteh-Gohari, M. and Habibi-Yangjeh, A. (2016). Ultrasonic-assisted preparation of novel ternary ZnO/AgI/Fe 3 O 4 nanocomposites as magnetically separable visible-light-driven photocatalysts with excellent activity. *Journal of Colloid and Interface Science*, 461, pp.144-153.

Shekofteh-Gohari, M. and Habibi-Yangjeh, A. (2017). Combination of CoWO 4 and Ag 3 VO 4 with Fe 3 O 4 /ZnO nanocomposites: Magnetic photocatalysts with enhanced activity through p-n-n heterojunctions under visible light. *Solid State Sciences*, 74, pp.24-36.

Shekofteh-Gohari, M. and Habibi-Yangjeh, A. (2017). Fe3O4/ZnO/CoWO4 nanocomposites: Novel magnetically separable visible-light-driven photocatalysts with enhanced activity in degradation of different dye pollutants. *Ceramics International*, 43(3), pp.3063-3071.

Shivaramu, P., Patil, A., Murthy, M., Tubaki, S., Shastri, M., Manjunath, S., Gangaraju, V. and Rangappa, D. (2017). Magnetic substrate supported ZnO-CuO nanocomposite as reusable photo catalyst for the degradation of organic dye. *Materials Today: Proceedings*, 4(11), pp.12314-12320.

Shylesh, S., Schünemann, V. and Thiel, W. (2010). Magnetically Separable Nanocatalysts: Bridges between Homogeneous and Heterogeneous Catalysis. *Angewandte Chemie International Edition*, 49(20), pp.3428-3459.

Sin, J., Lam, S. and Mohamed, A. (2010). Optimizing photocatalytic degradation of phenol by TiO2/GAC using response surface methodology. *Korean Journal of Chemical Engineering*, 28(1), pp.84-92.

Sin, J., Lam, S., Lee, K. and Mohamed, A. (2013). Photocatalytic performance of novel samarium-doped spherical-like ZnO hierarchical nanostructures under visible light irradiation for 2,4-dichlorophenol degradation. *Journal of Colloid and Interface Science*, 401, pp.40-49.

Sin, J., Lam, S., Lee, K. and Mohamed, A. (2013). Self-assembly fabrication of ZnO hierarchical micro/nanospheres for enhanced photocatalytic degradation of endocrine-disrupting chemicals. *Materials Science in Semiconductor Processing*, 16(6), pp.1542-1550.

Sin, J., Lam, S., Mohamed, A. and Lee, K. (2012). Degrading Endocrine Disrupting Chemicals from Wastewater by Photocatalysis: A Review. *International Journal of Photoenergy*, 2012, pp.1-23.

Souza, R., Freitas, T., Domingues, F., Pezoti, O., Ambrosio, E., Ferrari-Lima, A. and Garcia, J. (2016). Photocatalytic activity of TiO2, ZnO and Nb2O5 applied to degradation of textile wastewater. *Journal of Photochemistry and Photobiology A: Chemistry*, 329, pp.9-17.

Sun, H., Yu, Y., Luo, J., Ahmad, M. and Zhu, J. (2012). Morphology-controlled synthesis of ZnO 3D hierarchical structures and their photocatalytic performance. *CrystEngComm*, 14(24), p.8626.

Sun, L., Wu, W., Yang, S., Zhou, J., Hong, M., Xiao, X., Ren, F. and Jiang, C. (2014). Template and Silica Interlayer Tailorable Synthesis of Spindle-like Multilayer α-Fe2O3/Ag/SnO2Ternary Hybrid Architectures and Their Enhanced Photocatalytic Activity. *ACS Applied Materials & Interfaces*, 6(2), pp.1113-1124.

Suresh, S. and Karthikeyan, S. (2016). Optical, magnetic and photocatalytic properties of magnetically separable Fe3O4-doped ZnO and pristine ZnO nanospheres. *Journal of the Iranian Chemical Society*, 13(11), pp.2049-2057.

Tabasideh, S., Maleki, A., Shahmoradi, B., Ghahremani, E. and McKay, G. (2017). Sonophotocatalytic degradation of diazinon in aqueous solution using iron-doped TiO 2 nanoparticles. *Separation and Purification Technology*, 189, pp.186-192.

Thennarasu, G. and Sivasamy, A. (2016). Enhanced visible photocatalytic activity of cotton ball like nano structured Cu doped ZnO for the degradation of organic pollutant. *Ecotoxicology and Environmental Safety*, 134, pp.412-420.

Tokode, O., Prabhu, R., Lawton, L. and Robertson, P. (2016). Controlled periodic illumination in semiconductor photocatalysis. *Journal of Photochemistry and Photobiology A: Chemistry*, 319-320, pp.96-106.

Vaiano, V., Matarangolo, M., Murcia, J., Rojas, H., Navío, J. and Hidalgo, M. (2018). Enhanced photocatalytic removal of phenol from aqueous solutions using ZnO modified with Ag. *Applied Catalysis B: Environmental*, 225, pp.197-206.

Vinod, R., Junaid Bushiri, M., Achary, S. and Muñoz-Sanjosé, V. (2015). Quenching and blue shift of UV emission intensity of hydrothermally grown ZnO:Mn nanorods. *Materials Science and Engineering: B*, 191, pp.1-6.

WANG, H., XIE, C., ZHANG, W., CAI, S., YANG, Z. and GUI, Y. (2007). Comparison of dye degradation efficiency using ZnO powders with various size scales. *Journal of Hazardous Materials*, 141(3), pp.645-652.

Wang, J., Yang, J., Li, X., Wang, D., Wei, B., Song, H., Li, X. and Fu, S. (2016). Preparation and photocatalytic properties of magnetically reusable Fe3O4@ZnO core/shell nanoparticles. *Physica E: Low-dimensional Systems and Nanostructures*, 75, pp.66-71.

Wang, X., Yu, J., Ho, C., Hou, Y. and Fu, X. (2005). Photocatalytic Activity of a Hierarchically Macro/Mesoporous Titania. *Langmuir*, 21(6), pp.2552-2559.

Wang, Z., Cai, W., Hong, X., Zhao, X., Xu, F. and Cai, C. (2005). Photocatalytic degradation of phenol in aqueous nitrogen-doped TiO2 suspensions with various light sources. *Applied Catalysis B: Environmental*, 57(3), pp.223-231.

Wei, Y., Han, B., Hu, X., Lin, Y., Wang, X. and Deng, X. (2012). Synthesis of Fe3O4 Nanoparticles and their Magnetic Properties. *Procedia Engineering*, 27, pp.632-637.

Wei, Y., Han, B., Hu, X., Lin, Y., Wang, X. and Deng, X. (2012). Synthesis of Fe3O4 Nanoparticles and their Magnetic Properties. *Procedia Engineering*, 27, pp.632-637

Whiteley, A. and Bailey, M. (2000). Bacterial Community Structure and Physiological State within an Industrial Phenol Bioremediation System. *Applied and Environmental Microbiology*, 66(6), pp.2400-2407.

Wu, C., Liu, X., Wei, D., Fan, J. and Wang, L. (2001). Photosonochemical degradation of Phenol in water. *Water Research*, 35(16), pp.3927-3933.

Xia, J., Wang, A., Liu, X. and Su, Z. (2011). Preparation and characterization of bifunctional, Fe3O4/ZnO nanocomposites and their use as photocatalysts. *Applied Surface Science*, 257(23), pp.9724-9732.

Xie, S., Zhang, Q., Liu, G. and Wang, Y. (2016). Photocatalytic and photoelectrocatalytic reduction of CO2 using heterogeneous catalysts with controlled nanostructures. *Chemical Communications*, 52(1), pp.35-59.

Xu, J., Ao, Y. and Chen, M. (2009). Preparation of B-doped titania hollow sphere and its photocatalytic activity under visible light. *Materials Letters*, 63(28), pp.2442-2444

Yang, K., Peng, H., Wen, Y. and Li, N. (2010). Re-examination of characteristic FTIR spectrum of secondary layer in bilayer oleic acid-coated Fe3O4 nanoparticles. *Applied Surface Science*, 256(10), pp.3093-3097.

Yang, L., Dong, S., Sun, J., Feng, J., Wu, Q. and Sun, S. (2010). Microwave-assisted preparation, characterization and photocatalytic properties of a dumbbell-shaped ZnO photocatalyst. *Journal of Hazardous Materials*, 179(1-3), pp.438-443.

Yasmina, M., Mourad, K., Mohammed, S. and Khaoula, C. (2014). Treatment Heterogeneous Photocatalysis; Factors Influencing the Photocatalytic Degradation by TiO2. *Energy Procedia*, 50, pp.559-566.

Ye, J., Li, X., Hong, J., Chen, J. and Fan, Q. (2015). Photocatalytic degradation of phenol over ZnO nanosheets immobilized on montmorillonite. *Materials Science in Semiconductor Processing*, 39, pp.17-22.

Yu, J., Xiang, Q. and Zhou, M. (2009). Preparation, characterization and visible-light-driven photocatalytic activity of Fe-doped titania nanorods and first-principles study for electronic structures. *Applied Catalysis B: Environmental*, 90(3-4), pp.595-602.

Zangeneh, H., Zinatizadeh, A., Habibi, M., Akia, M. and Hasnain Isa, M. (2015). Photocatalytic oxidation of organic dyes and pollutants in wastewater using different modified titanium dioxides: A comparative review. *Journal of Industrial and Engineering Chemistry*, 26, pp.1-36.

Zhang, J., Shen, H., Wang, X., Wu, J. and Xue, Y. (2004). Effects of chronic exposure of 2,4-dichlorophenol on the antioxidant system in liver of freshwater fish Carassius auratus. *Chemosphere*, 55(2), pp.167-174.

Zhao, Y., He, Y., Xiong, D., Ran, W., Liu, Z. and Gao, F. (2014). Dual template synthesis and photoelectrochemical performance of 3-D hierarchical porous zinc oxide. *International Journal of Hydrogen Energy*, 39(25), pp.13486-13490.

Zhong, W., Wang, D., Xu, X., Luo, Q., Wang, B., Shan, X. and Wang, Z. (2010). Screening level ecological risk assessment for phenols in surface water of the Taihu Lake. *Chemosphere*, 80(9), pp.998-1005.

Zhu, L., Ghosh, T., Park, C., Meng, Z. and OH, W. (2012). Enhanced Sonocatalytic Degradation of Rhodamine B by Graphene-TiO2 Composites Synthesized by an Ultrasonic-Assisted Method. *Chinese Journal of Catalysis*, 33(7-8), pp.1276-1283.